Universidade Federal do Rio Grande do Sul
Institudo de Física
Departamento de Astronomia

StarHorse: A Bayesian tool for determining masses, ages, distances and extinction for field stars

Anna Bárbara de Andrade Queiroz

Msc. dissertation taken under the supervision of Dr. Basílio Xavier Santiago submitted to the Graduate Program of *Instituto de Física - Universidade Federal do Rio Grande do Sul* (UFRGS) as part of the fulfilment to obtain the master's degree in physics with emphasis in astrophysics.

Porto Alegre, RS, Brasil
May of 2018

* This work has received financial support from Conselho Nacional de Desenvolvimento Científico e Tecnológico (CNPq)

Universidade Federal do Rio Grande do Sul
Institudo de Física
Departamento de Astronomia

StarHorse: uma ferramenta Bayesiana para determinação de massas, idades, distâncias e extinção para estrelas de campo

Anna Bárbara de Andrade Queiroz

Porto Alegre, RS, Brasil
Maio de 2018

⋆ Trabalho financiado pelo Conselho Nacional de Desenvolvimento Científico e Tecnológico (CNPq)

"And if you're frightened
You can be frightened
You can be, it's ok"
Radiohead
(My Iron Lung, The Bends 1995.)

Acknowledgements

To my mother, Neusa Maria de Andrade who gave me the best example of how a strong a woman can be, who also taught me to never gave up on my dreams, and most importantly, who was an incredible father and mother to me and my brothers even with the few resources life offer to her.

To my advisor, Basílio Xavier Santiago, who has been advising me since the beginning of the under-graduation course, for all the teachings, patience, understandings, recognition, trust, and efforts done to my growth as a scientific researcher.

To Cosmos, a very special cat, which is always biting and purring at me, especially when he knows I need.

To Friedrich Anders, who directly shares with me the development of StarHorse, for sharing with me amazing and crazy ideas, for all support, and most importantly for being my friend.

To Christina Chiappini, my future advisor, for giving me the chance to show my potential, for the amazing advising and collaboration during this work, and also to be this great example of a woman in science.

To all of my friends, who are always encouraging my work and me to be a better person, to always stand out for me, and for simply being in my life. Christian Herez, Friedrich Anders, Gabriela Tomaz, Ingrid Pelisoli, Ivanessa Almansa, Jonas Pereira, Lais Gedoz, Larissa Amaral, Marina Dal Ponte, Monica Tergolina, Nicolas Mallmann, Paulo Casagrande, Samantha Alixandrino. I especially appreciate for those who helped me in this hard moment of life, which was to write this dissertation after a complicated breakup. It would be a hundred times harder without their help.

To the support of all my family, to my brother Rafael Golçalves, to my grandmother Edith Queiroz and to my father Renato Queiroz.

To all the Professors of the physics institute and of the astronomy department, especially to Alan Alvez Brito, Alejandra Romero, Ana Chies Santos, Basílio Santiago, and Horacio Dottori. Who, during this masters, gave me wonderful classes,

research and life advice.

To the examining board of this dissertation, for accepting the invitation to analyse this work.

Abstract

We are in an advantageous position to study the formation and evolution of disk galaxies. By being inside the Milky Way, we are able to make detailed observations about the individual stars that compose it. With the technological revolution of the latest years, it has been possible to collect a massive set of information, (e.g. chemical composition, kinematics, astrometry, and atmospheric parameters), with high resolution for a large portion of the Galactic volume. With the goal to understand better our Galaxy, we developed a tool, called `StarHorse`, that can estimate distances, ages, masses, and extinction from the available spectroscopic, astrometric, and photometric information. `StarHorse` makes these estimates through a Bayesian method, that builds a probability distribution over the models by calculating a likelihood function between observation and stellar evolution models, and by using common knowledge about our Galaxy as priors. The parameters that StarHorse estimates are crucial to Galactic archaeology studies. With them, we can investigate the structure, the star formation history, the initial mass function, the three-dimensional dust map of our Galaxy, and provide constraints to chemodynamical models of the Milky Way. In this work, we focus on the description and validation of the method, testing its applicability in recent spectroscopic and astrometric surveys. We also make available catalogs with distances and extinctions to the astronomy community. Our distances and extinctions became a reference inside the APOGEE-team and were released as part of the SDSS Data Release 14. Moreover, we made available catalogs also to other spectroscopic surveys such as Gaia-ESO, RAVE, and GALAH. In this work, we also explore these results, especially for APOGEE, in a broad Galactic archaeology context.

Key-words: Stars: distances – fundamental parameters – statistics; Galaxy: stellar content.

Resumo

Nos encontramos em uma localização vantajosa para o estudo da formação e evolução de galáxias espirais. Situados no disco da Via-Láctea, somos capazes de fazer observações detalhadas sobre as estrelas individuais que a compõem. Com o avanço tecnológico das últimas décadas, foi possível coletar um grande conjunto de informações, (*e.g.* composição química, cinemática, astrometria e parâmetros atmosféricos), com alta resolução para uma vasta parte do volume Galáctico. Com o objetivo de compreender melhor a nossa Galáxia, desenvolvemos uma ferramenta, chamada `StarHorse`, que estima parâmetros como distâncias, idades, massas e avermelhamento utilizando informação disponível em levantamentos espectroscópicos, fotométricos e astrométricos. O código `StarHorse` estima os parâmetros através de um método Bayesiano, que constrói uma distribuição de probabilidade a partir do cálculo de verossimilhança entre observações e modelos de evolução teórica e a partir de priores Galácticos bem conhecidos. Os parâmetros que o `StarHorse` estima são cruciais para estudos de arqueologia Galáctica. Com eles é possível investigar a estrutura, o histórico de formação estelar, a função de massa inicial, o mapa tridimensional da nossa Galáxia e também adicionar vínculos a modelos quemodinâmicos da Via Láctea. Neste trabalho, focaremos na descrição e validação do método, testando sua aplicabilidade em levantamentos recentes de espectroscópica, astrometria e fotometria. Também disponibilizamos catálogos com distâncias e extinção para comunidade astronômica. As nossas distâncias e extinções se tornaram referência dentro da colaboração APOGEE e foram liberadas junto com o seu *Data Release* 14. Ademais, catálogos foram liberados para os *surveys* RAVE, Gaia-ESO e GALAH. Neste trabalho, exploramos os resultados do `StarHorse`, especialmente os resultados APOGEE, em um contexto amplo de arqueologia Galáctica.

Palavras-Chave: Estrelas: distâncias – parâmetros fundamentais – estatística; Galáxia: conteúdo estelar.

Notation

The following abbreviations, acronyms, symbols, and units are used throughout this dissertation:

$[M/H]$ - Overall Metallicity

2MASS - Two-Micron All-Sky Survey

ΛCDM - Λ Cold Dark Matter paradigm

π - Parallax

τ - Age

AIP - Leibniz-Institut für Astrophysik Potsdam

AMR - Age Metallicity Relation

APOGEE - Apache Point Observatory Galactic Evolution Experiment

d - Distance

ELS - Eggen, Lyndenbell, Sandage model (1962)

GALAH - Galactic Archaeology with HERMES

GES - Gaia-ESO

Gyr - Giga years, 10^9 years

HB - Horizontal Branch

HRD - Hertzsprung Russell Diagram

IMF - Initial Mass Function

ISM - Interstellar Medium

kpc - kilo Parsecs

LEGUE - LAMOST Experiment for Galactic Understanding and Exploration

LIneA - Laboratório In-terinstitucional de e-Astronomia

logg - Logarithmic Superficial Gravity

mag - magnitude

MARVELS - Multi-object APO Radial-Velocity Exoplanet Large-area Survey

MSTo - Main Sequence Turn-off

MW - Milky Way

NIR - Near-Infrared

pc - Parsecs

RAVE - Radial Velocity Experiment

RGB - Red Giant Branch

SDSS - Sloan Digital Sky Survey

SEGUE - Sloan Extension for Galactic Understanding and Exploration

SFR - Star Formation Rate

T_{eff} - Effective Temperature

VAC - Value Added Catalogue

Contents

List of Figures

Chapter 1

Introduction

How do galaxies form and evolve is a key question in astrophysics. Even with the progress of the last decades, this problem is still not entirely solved and is very important for unravelling the theories about the beginning of the Universe. The most common type of galaxies in the local Universe are dwarf elliptical galaxies, although disk galaxies, such as the Milky-Way, are more common amongst the luminous galaxies (**??**). Contrary to elliptical galaxies, disk galaxies, are characterised by an ordered motion of most of the stars forming a plane with spiral arms. About half of spiral galaxies do present a central linear bar. Barred spiral galaxies are classified as SBs according to the Hubble sequence, see Figure **??**. The central bulge becomes less important from Sa to Sc and the arms more open and likely to contain a larger fraction of gas and star-forming regions (**?**). Although we cannot see a flat projection of the Milky Way, it has been shown that it presents a central bar (**?**) and its classification should be of a SBc galaxy (**?**).

To investigate the formation and evolution of galaxies we can study other galaxies at different redshifts, (**??**), therefore observing them at different times of evolution. However, studying the Milky Way presents unique aspects that can help us to understand spiral galaxies in general. The Milky Way is the only galaxy where we can study large samples of individual stars, both using photometry and spectroscopy, at high S/N with high spectral resolution. For Milky-Way stars we are able to extract detailed information, such as distances and spatial velocities (i.e., phase space positions), detailed chemical abundances and atmospheric parameters. When combining these parameters, we can trace the past history of the Milky Way. For that reason our Galaxy plays a crucial role in studies of resolved stellar populations in disk galaxies, or in galaxies in general.

In this work, we focus on the study of Galactic archaeology, which is the study of the

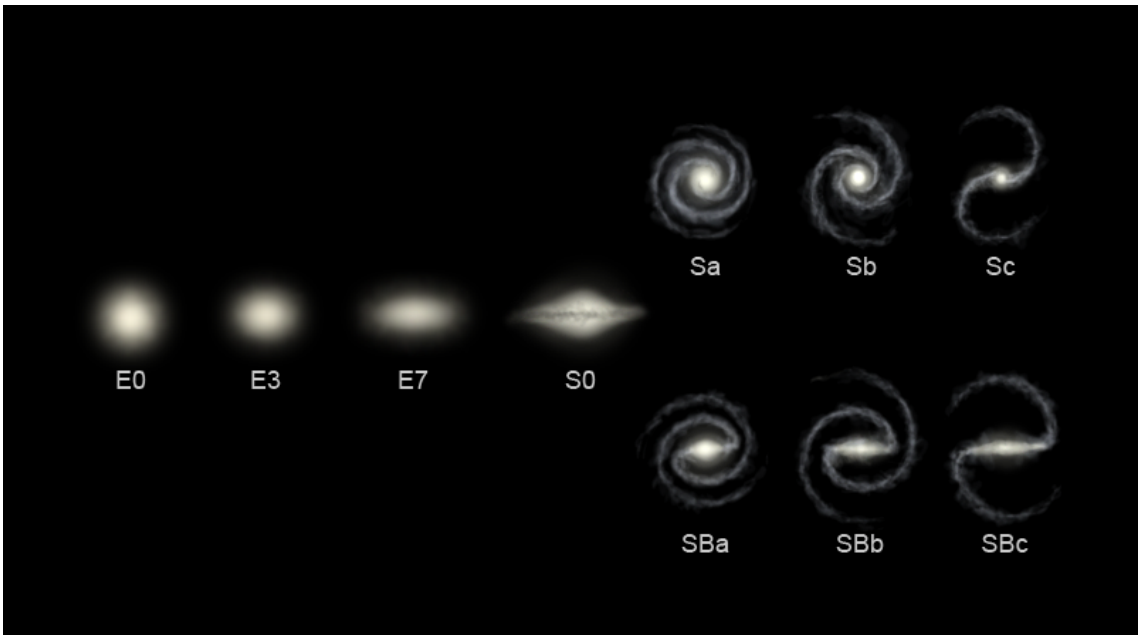

Figure 1.1: Galaxy classification determined by Edwin Hubble in 1936. At the left side of the figure we see the elliptical galaxies and in the right side are the spiral galaxies and barred spiral galaxies. Image was taken from `https://es.wikipedia.org/wiki/Secuencia_de_Hubble` accessed April 26th of 2018

structure, formation and evolution of our Galaxy. For that propose we developed a code called `StarHorse` that can estimate distances, ages, masses and extinction from available photometry and spectroscopy of individual stars. In the next sections we explain in more detail what we know about the Milky Way and how we can improve this knowledge with `StarHorse`.

1.1 Milky Way Structure and populations

The Milky Way is our home in the Universe. We can see it in a dark night as a band of light crossing the sky. This band of light is made up of billions of stars, dust and gas held together by gravitational attraction. The stellar mass of our Galaxy is around $8.5 \times 10^{10} M\odot$, and virial mass of $1.3 \times 10^{12} M\odot$ (**?**). It is the second most massive galaxy in the Local Group, second to Andromeda, which is also a spiral galaxy (**?**). Besides that, our Galaxy, and probably all galaxies, is surrounded by dark matter halo, which is an unknown form of matter that interacts with the baryonic matter only gravitationally (**?**). The Milky Way is a barred spiral galaxy, see Figure **??**. It consists of a triaxial central bulge, with a linear bar, a disk with spiral arms and a diffuse extended spheroid, called halo, with several globular

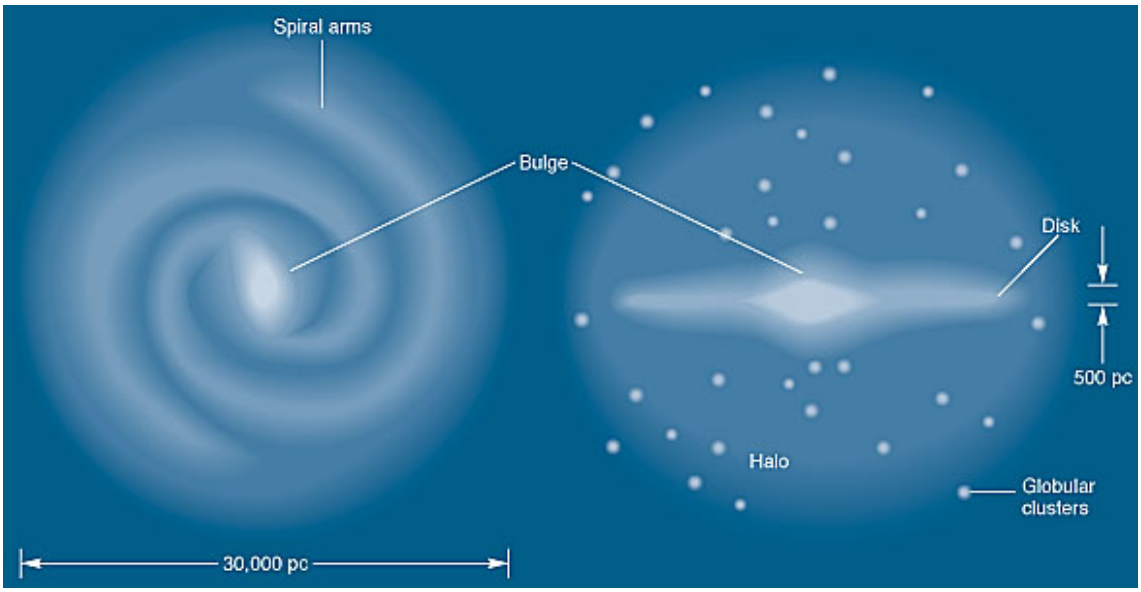

Figure 1.2: Sketch of Milky Way from edge on and flat projections. The sketch shows the central bulge, spiral arms, the disk and the halo. Image was taken from `https://astrobob.areavoices.com/2014/06/01/beautiful-m5-globular-cluster-will-send-shivers-down-your-spine/` accessed 27th of April of 2018

clusters in it. The solar system is located in the Galaxy's disk, around 8 kpc from the Galactic center (**?**).

A historical picture of the Milky Way formation, describing its individual structural components, date as far back as the 1960s **?**) (ELS). Back then the model of ELS discribed the formation of the halo and disk as a monolithic collapse, the halo being formed first in a short timescale, yielding high eccentricity stellar orbits and a negative metallicity gradient. The disk would then have formed over much longer timescales by a dissipative process of infalling of high angular momentum gas. The discovery of metal-poor disk stars with disk kinematics and the large range of metal abundances of halo globular clusters, independent of direction, were later observational evidences that challenged this paradigm (**?????**). These observations suggested that the halo was built up from infalling fragments (**?**). More recent models, are inspired by the current Λ Cold Dark Matter paradigm (ΛCDM), which is a model that comprehends cosmological observations as the large scale structure formed by the distribution of galaxies, the existence of the cosmic microwave background and the accelerating expansion of the universe (**???**). These models predict that structure formation of galaxies is in general hierarchical, with large structure forming by the merging of smaller ones. One of the observational evidences, that

corroborates the hierarchical model, is the detection of unrelaxed substructures that are being tidally disrupted by Milky Way (MW) gravitational potential (**???**). A relatively large and luminous spiral such as the MW, in this context, has formed from thousands of sub-Galactic fragments, likely dark-matter rich ones, in a process that is quite distinct from the ELS monolithic collapse model. In this contemporary picture of Galaxy formation, different and yet relatively unconstrained scenarios for the disk, bulge and halo formation have been invoked. In the next subsections we explain in more detail the characteristics of each MW component, and what the more recent observational facts suggests about the Milky Way formation and evolution.

1.1.1 Bulge

The bulge is the central component of our Galaxy as shown in Figure **??**. Due to the highly variable extinction in the direction of the bulge, studying its stars has been very challenging to astronomers, and this component was left out from the first theories of evolution and formation of the Milky Way (**??**). Bulge stars have in general been studied through the Baade's window, which is a low extinction gap in the bulge direction (e.g. **???**), through infrared photometric surveys (e.g. **??**), and through microlensing events (e.g. **???**). Bulge stars are in general old, ($\tau > 10 Gyrs$) (**??**), though recent surveys have shown that the bulge presents young populations located in the plane (**??**). This age distribution favours a scenario of bulge formation from disk instabilities, though these young populations can be contamination from disk stars due to the uncertain distances and difficulties of having bona-fied bulge samples. The selection of cleaner bulge samples is of paramount importance for a proper bulge analysis. Therefore, every time we refer to "the bulge", we should have in mind that contamination by other Galactic components might be an issue. The metallicity distribution of bulge is broad, ranging from $-3 < [Fe/H] < +1\ dex$, with a vertical gradient (**??**), with high metallicity stars closer to the plane. This gradient was first interpreted to result of a formation scenario from accretion via mergers or dissipational collapse (**?**), but **??**) showed that the metallicity gradients are a natural consequence of a bulge formed by disk instabilities. The structure of the bulge was first thought to be spherical, but with near-infrared photometry observation from COBE-DIRBE (**?**) and from star counts of the 2MASS survey (**?**) it was shown that the bulk of the stars in the bulge are part of a box-peanut structure, (**??**) later also confirmed by the VVV survey (**?**). This is consistent with the observed kinematics that show cylindrical rotation (**??**). Models of a triaxial bulge are listed in **?**) where the best fit to 2MASS data is described by density profiles of $sech^2$.

Amongst the several possible scenarios for bulge formation, the scenario of formation by disk and bar buckling instabilities can explain the vertical metallicity gradient, the box-peanut shape and its predominant old age, which implies an inside-out disk formation. However, there is not yet a chemodynamical model that can fully describe the bulge. To better constrain these models, it is still necessary to improve the 3D map of chemical composition, kinematics and age information of bulge field stars (see **?**) for further discussions on this matter).

1.1.2 Disk

Outside the bar/bulge structure, stars are mainly located in a flat plane called the disk of the Galaxy. The disk contains four spiral arms (**?**), and it is on the spiral arms that most of the interstellar medium (ISM), made up of gas and dust, is contained. Therefore, this is also where star-forming regions are usually found. In Figure **??** we can see a scheme of the spiral arms projected into Galactic coordinates, with the Sun in the center.

Although our location in the Galaxy gives us the advantage to study stellar populations with unique information and detail, there are also some disadvantages in our location. The Solar System is inside the disk between two spiral arms, the Perseus arm and the Sagittarius arm. This position hinders observations of the inner bulge and the outer disk, because extinction is very high towards these directions. The first detailed studies of the stellar disk used simple models to project star counts in a given photometric band (**?**) towards several different directions. According to this model, the dominant disk is thin, with a double exponential law in directions parallel and perpendicular to the plane (with a scale length of $h_R \simeq 2.5$ kpc and a scale height of $h_z \simeq 0.3$ kpc for older stars, and $h_z \simeq 0.1$ kpc for most of the ISM and young stars). Some years later, **?**), also using star counts towards the Galactic North pole showed that the distribution of disk stars perpendicular to the plane requires two exponential laws instead of a single one. And in an analysis of the number density profile of the photometry from Sloan Digital Sky Survey (SDSS), **?**) fitted these two exponential laws with scale heights of $h_z \simeq 0.3$ kpc for the thin disk and $h_z \simeq 0.9$ kpc for the thick disk. The properties of the thin and thick disks have since then been subject to many studies and reviews (**?????**). The existence of a thick disk is ubiquitously found in external disk galaxies as well (**???**). Until recent years, the detailed analyses of the thin and thick disk stellar populations were largely restricted to the solar neighborhood or to the system of open and globular clusters. The thin disk is known to harbor almost all of the

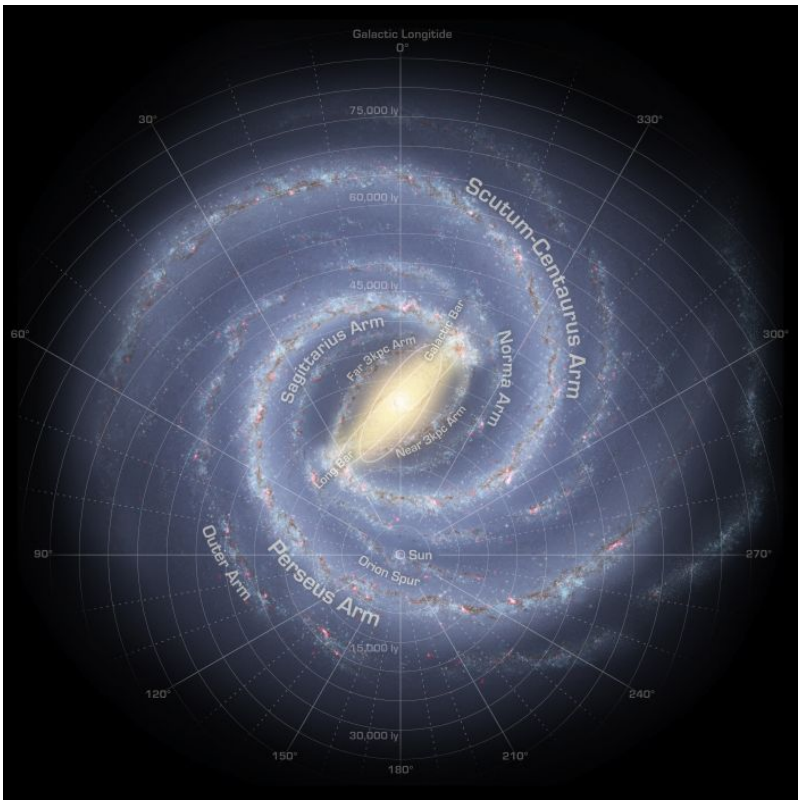

Figure 1.3: Scheme of the Milky Way spiral arms, projected into Galactic coordinates with the Sun in the center. There are two main spiral arms, the Centaurus arm and the Perseus arms, and two minor arms, the Sagittarius and Norma arm. The Sun is located between the Perseus and Sagittarius arm. Image was taken from `http://www.solstation.com/x-objects/cenbulge.htm` accessed 4th of May of 2018

ISM and for that reason, it is the component where essentially all star formation is currently going on. Therefore, young populations are concentrated in the thin disk, which is dynamically cold, since the velocity dispersion of a disk population increases with age (**????**). The dependence of velocity dispersion with age can be explained by gravitational field variations with time, resulting in a more perturbed orbit for older stars. The thin disk is dominated by differential rotation ($V_{rot} \simeq 238$ km/s at the $R \simeq 8.33$ kpc solar circle and beyond, where R is a cylindrical coordinate on the disk plane, with origin in the Galactic center) and with small radial and vertical velocity dispersion ($\simeq 35$ km/s and $\simeq 25$ km/s) respectively. The thick disk is older and consequently characterized by a larger vertical and radial velocity dispersion ($\simeq 50$ km/s). The thick disk locally has a lag velocity of $\simeq 50 - 70$ km/s with respect to the local standard of rest (and hence $V_{rot} \simeq$ 150-170 km/s) (**?**). Recently **???**) doubted the existence of the thick disk as an independent structure, by taking into account the observational selection function of the specific surveys and analysing the structures of mono-abundance and mono-age populations. They found a continuously varying spatial distribution as different mono-abundance (or mono-age and mono-abundance) populations were separately studied. However, **?**) shows that the mono-abundance does not correspond to mono-age populations. Thick disk stars make up about 20% of the stars around the Sun (roughly at $z \simeq 0$, where z is the vertical cylindrical coordinate). Its member stars also differ from the thin disk stars for being relatively old (**??**) ($\tau \simeq 10$ *Gyrs*, compared to the large age span of the thin disk, where 10 *Gyr* is basically an upper limit) (**?????**). Thin and thick disk stars can also be distinguished by their chemical composition. High-resolution spectra of thick disk stars in the solar neighbourhood showed that thick disk stars have higher abundance of α-elements in respect to iron abundance, $[\alpha/Fe]_{Thick} > [\alpha/Fe]_{thin}$ (**????**). This separation can be clearly seen as a gap in the $[\alpha/Fe] - [Fe/H]$ plane, even for large Galactic radius see **????**). This different chemical signature of the thick and thin disk could suggest these components were formed at different times as first suggested by the so-called Two-Infall model scenario (**?**). The thick disk, for instance, may have been born kinematically hot, from large gas accretion rates that were typical in the early Universe (**??**). A second scenario would be a thick disk created through accretion of Galaxy satellites or through the heat of a pre-existing thin disk by mergers (**?**). Alternatively the thick disk could also have been formed by radial migration (**?**). As emphasized by previous authors (see **?**) for a historical account), the prescription for Galaxy formation involves not only achieving a state of dynamical equilibrium in the the dark matter-

dominated Galactic potential, but also of the processes governing baryonic matter, including: i) the rate at which gas is converted in stars through time (the star formation rate, SFR(t)); ii) the rate at which the ISM (and the stars formed from it at any given time) evolves chemically (often quantified by a simple age-metallicity relation, AMR); iii) the efficiency with which the material processed inside stars and returned back to the ISM is mixed; iv) the feedback from violent processes such as supernovae explosions, nuclear activity; v) the amount of fresh gas is accreted to the forming Galaxy. Equally important are dynamical processes that transfer stars from their birth places. The most striking such process is Galactic cannibalism, by which a dwarf galaxy, such as the Sagittarius Dwarf, is accreted to the MW, mixing its previously formed member stars to those of the MW halo. But more subtle processes, such as radial migration may also be in place, specially in the Galactic disk (**??**).

1.1.3 Halo

The Galactic halo is a nearly spherical component that surrounds the disk and the bulge, see Figure **??**. The halo is sparsely populated by field stars and globular clusters, it contains only about 1% of the total MW stellar mass. At larger Galactic radii ($\simeq$ 100 kpc), the Galactic halo is completely dominated by dark matter, having a virial radius of $\simeq$ 250 kpc (**?**). Given the small number of halo member stars passing by the Solar vicinity, most of what we knew about the Galactic halo, until recently, came from deep pencil-beam star counts at high-Galactic latitudes or studies of the globular cluster system. The MW globular cluster system, for instance, contains two subpopulations: one is metal-richer and has a disk-like kinematics, while the other, more metal-poor, is the one associated to the halo (**?**). Among the halo clusters, horizontal branch morphology further divides the system between blue and red horizontal branches (**?**). In the halo, a considerable number of MW satellites are also found, most of them ultra-faint dwarf spheroidal (e.g. **???**), as well as some star clusters (e.g. **???**). Both types of stellar systems extend as far as, or even beyond, the virial radius. Most of what we know about the stellar halo comes from studies of these stellar systems (**????**). Stellar streams are also found in the halo, either associated to known dwarf galaxies and globular clusters (**??**), or not (**??**). Field stars tracing the halo have also been studied, but usually at closer distances (**????**) and involving stars belonging to the halo (old) main-sequence turn-off. More luminous halo tracers also include horizontal branch stars (**??**), as well as RGB stars (**?**). Based on these analyses, the structure of the halo is often described as a double

power-law, with slopes $\simeq 2.5$ and $\simeq 3.7$ for radii smaller (larger) than $\simeq 25$ kpc (**?**). Halo stars have low metallicity and enhanced alpha elements suggesting that these stars formed relatively early in the Universe (**??**). There is observational evidence for a dual halo with metallicities peaking at $\simeq -1.6$ and $\simeq -2.2$ (**???**). The recent *Gaia* Data Release two, has also shown two distinct populations in the observational HR-diagrams for halo stars, see **?**). Some evidence also has been found for a metallicity gradient at the inner parts of the Galactic halo, and a small negative age gradient with distance from the Galactic plane of $\simeq -13.9$ Myr/kpc and age gradient with radial Galactocentric distance of $\simeq -25.9$ (**?**). Such inhomogeneous halo, in contrast to a smooth one, has been one of the main results in favour of a hierarchical scenario of structure formation. On the other hand, even today there is some debate if whether the current census of MW satellites match the expected numbers from ΛCDM cosmology, something that has traditionally been coined as the *Missing satellite problem* (**??**). The dark matter hierarchical clustering simulations, do not match well the number of dwarf galaxies expected. The expected number of dwarf galaxies is orders of magnitude lower than the observed number.

1.2 Large Stellar Surveys

Recent years have witnessed an exponential increase in the amount of data on Galactic stellar populations. This largely stems from the increase in computational power coupled with advances in telescope and detector technology. Both have allowed large photometric and spectroscopic surveys to be carried out, whose collected data are then reduced by means of streamlined sets of routines (making up a *pipeline*). Pioneering among the imaging surveys are, the Sloan Digital Sky Survey (SDSS, **?**), which is already in its fourth phase SDSS-IV (**?**), and the Two-Micron All-Sky Survey (2MASS, **?**). These surveys have collected magnitudes and colors from millions of stars in the optical and near infra-red (NIR), respectively. Dating back from the late 1990's and early 2000's, these surveys, among other things, have revealed a highly substructured stellar halo, harboring dozens of previously undetected faint star clusters, dwarf galaxies and stellar streams (**????**). This has allowed a closer investigation into hierarchical models mentioned in Section **??**. These surveys also revealed, with star counts, the structure of the bulge and the thin/thick disks (**??**) as mentioned in Section **??** and in Section **??**. Thanks to 2MASS NIR photometry, it was possible to uncover the central regions of the Galaxy as never before, confirming the MW to be a barred spiral and allowing for more detailed models for the

structure of the Galactic bulge (**?**). In the past decade, SDSS moved its focus from photometry to spectroscopy, adding a suite of stellar spectroscopic surveys, such as the Sloan Extension for Galactic Understanding and Exploration (SEGUE, **?**), The Multi-object APO Radial-Velocity Exoplanet Large-area Survey (MARVELS **?**), and the Apache Point Observatory Galactic Evolution Experiment (APOGEE, **?**). These surveys have a range of spectroscopic resolutions, and have covered a large amount of the Galactic volume, revolutionising our knowledge about the Milky Way. As explained in Section **??**, with spectroscopic information it was possible to better disentangle the thin and thick disks (**????**), as well as having an idea about their age distributions (**??**), consequently contributing for further constraints to chemical evolution models and chemodynamical models of the Milky Way (**???**). Other recent spectroscopic surveys include the Radial Velocity Experiment (RAVE **?**), the Gaia-Eso Survey (GES, **?**), the Galactic Archaeology with HERMES (GALAH, **?**), and the LAMOST Experiment for Galactic Understanding and Exploration (LEGUE, **?**). The combination of this spectroscopic information with photometry from SDSS, 2MASS, and APASS **?**) gives us a wealthy set of information about the stars that compose the Milky Way. In the last years all these spectroscopic surveys have increased the available spectroscopic samples by two orders of magnitude, covering in detail the Solar neighborhood, and reaching the bulge, the outer disk and halo stars. Most important of all, the recent data release 2 of the *Gaia* satellite **?**) contains astrometric solutions for near 1.7 billion stars, covering all the sky. *Gaia* is promising a big revolution in Galactic archaeology, delivering parallaxes, proper motions, and broadband photometry in optical wavelengths for this massive set of stars. This work focus especially on the APOGEE, RAVE, GES and GALAH spectroscopic surveys, for their medium to high-resolution spectra, sky coverage and wide use in the astronomy community. In Figure **??** we show the footprint of all these surveys put together. More detailed explanation of each survey and their use is given in Section 6. of Chapter **??**.

1.3 Why and how to obtain Distances, Ages, Masses and extinction?

This work is focused on the development and application of the `StarHorse` code, which is a tool that can estimates distances, ages, masses and extinction for field stars. `StarHorse` estimates these parameters with an input combination of available spectroscopic, astrometric and photometric surveys. In the two next subsections,

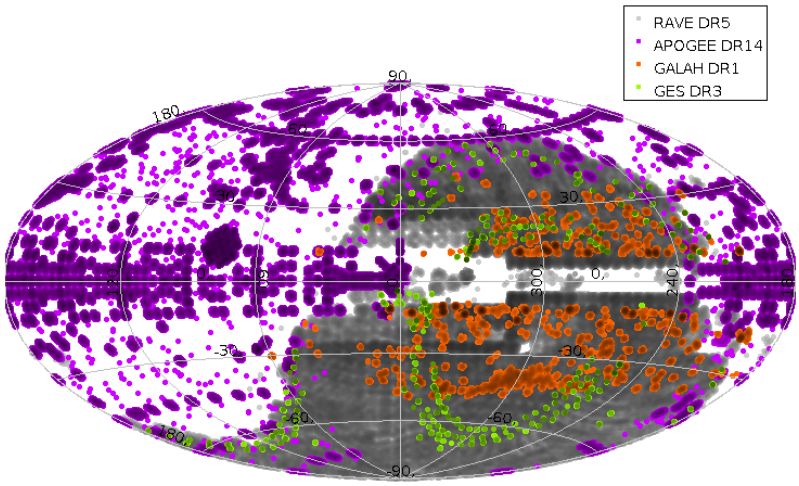

Figure 1.4: Aitoff projection showing each spectroscopic survey sky coverage. Credits: Anna Queiroz, 8th of May of 2018

we present the main motivations for developing this code and give a brief summary of it.

1.3.1 Motivations and scientific applications of `StarHorse`

As we have seen through Section **??** and Section **??** measuring distances, ages, masses and extinction for field stars is crucial for Galactic archaeology studies. Starting with distances, `StarHorse` will be extremely important for improving the distances given by *Gaia* parallaxes that reach the bulge, halo and outer disk. Stars in bulge region are obscured by extinction and are dim. At these distances, typical magnitudes of giant stars are $G > 17.0$, so that parallax uncertainties are ≈ 0.7 mas (**?**). Improving these distance estimates is going to be essential for the bulge and also for the inner Galaxy studies. Besides that, `StarHorse` can produce a whole 3D tomographic view of the Galaxy, holding a clear advantage over star counts studies which use counts as a function of the apparent magnitude and colour for different directions. Furthermore, the Bayesian approach also takes into consideration Galactic priors in a given direction and estimates the extinction alongside the distances. Distance estimations are necessary for orbital parameters determinations and rotational velocities. `StarHorse` (**??**) has already been welcomed by the community as shown by the several works which use our distances e.g. **???**). And with the increas-

ing spectroscopic and *Gaia* coverage `StarHorse` will be certainly needed for future chemodynamical studies of our Galaxy. A few other works have used `StarHorse` distances for studying the metallicity gradients and trends in the disk (**?????**) and also in the halo **??**). Recently `StarHorse` distances were also used to make kinematic confirmation of a stream near Segue 1 (**?**). `StarHorse` was also quoted by some of the *Gaia* Collaboration papers as an example of Bayesian approach needed to estimate better distances and extinctions (**???**).

Determining ages for field stars presents several challenges. The degeneracy in age between stellar evolutionary models is high since stars spend most of their time in the main sequence phase. To determine ages, we need very precise spectroscopic information and precise parallaxes to raise the high degeneracy between dwarf and giant stars. In general, ages have been determined by asteroseismology (**?????**), or by defining a sample of stars in the same evolutionary stage (**???**), which decreases the degeneracy between models. `StarHorse` ages are still prone to improvements and have been extensively tested through simulations and external validations (**?**). Age determination for field stars is essential in this era of Galactic archaeology (**?**), for unveiling a clearer and more detailed MW formation history. Only by gathering such information, along with chemical compositions and phase-space positions, we can finally compare this data with model predictions of MW formation and evolution. A first work using `StarHorse` ages is presented by (**?**), where ages are determined for a sample of FGK stars in the Solar neighbourhood with very high resolution. The work uses a dimensional reduction algorithm to tag stellar populations in abundance space and analyses each sub-population found. Future ages applications are expected for the increasing resolution in spectroscopic surveys and astrometric surveys such as *Gaia*.

Masses are important to reconstruct the Initial Mass Function (IMF) of field stars, while IMF analyses have often been restricted to the immediate Solar neighbourhood or to star clusters (**??**). Potentially, `StarHorse` mass estimates could help to reconstruct the field IMF and its possible spatial variations on the disk. However, extending IMF towards Galactic volumes larger than the Solar neighborhood would require assumptions about unresolved binaries.

1.3.2 `StarHorse` code

`StarHorse` is a `python` written code that applies a Bayesian statistical approach, where we compare a set of measured photometric, spectroscopic, and astrometric parameters to stellar evolutionary models to infer additional stellar parameters. some of which are present in these models. A complete set of measured parameters included in our method is {effective temperature, T_{eff} , surface gravity, $\log g$, overall metallicity $[M/H]$), photometric magnitudes, m_λ, and parallax, π}. The set of inferred parameters is {mass, m_*, age, τ, distance, d, and extinction (in V band, A_V)}. `StarHorse` applies this method building the posterior probability function with Parsec models (**?**). To a complete description of the Bayesian method, please check Chapter **??**, or see **??**). In Summary, `StarHorse` is a robust code, that can estimate distances, ages, masses and extinction for field stars. It is a choice flexible code, allowing the user to infer additional parameters for different sets of measured parameters. For example, the user can make estimates without parallax measurements, or even only using photometric measurements (the so-called *photometric parallaxes*). It also allows all photometric bands supported by the Parsec models and currently, the user can also choose between **?**) and **?**) extinction curves. In the era of *Gaia*, and of large spectroscopic surveys, `StarHorse` has to efficiently run over millions of stars, something that is only possible with the help of large computational clusters. We have made available value added catalogues (VACs) for a few spectroscopic surveys, see Section 6 of Chapter **??**, and we are recently executing `StarHorse` over a large data amount of *Gaia* DR2, for over a million targets, and for combinations of *Gaia* DR2 with spectroscopic surveys such as APOGEE, GALAH, and RAVE in computational clusters of the Leibniz-Institut für Astrophysik Potsdam (AIP, `http://www.aip.de/en`) and the Laboratório Interinstitucional de e-Astronomia (LIneA, `http://www.linea.gov.br/`) institutes.

Chapter 2

`StarHorse`: increasing the knowledge about our Galaxy

In this Section, we describe the code `StarHorse` and its validation, which relied on simulated spectrophotometric samples as well as on reference stellar samples with high confidence distance, reddening, mass and age estimates. Here we detailed the Bayesian method, the priors and the models that we apply, extensively testing the different options the code offers. We also present the application of `StarHorse` in a few spectroscopic catalogues, combined with photometry and astrometry information from *Gaia*. The results of these applications are made public for the community and it has already enabled a considerable number of scientific publications (**????**). We emphasise the importance of a Bayesian approach when using astrometric parallaxes from *Gaia*, as well mentioned by *Gaia* collaboration papers **?**), that also quote our code (**?**). `StarHorse` has as the main goal, to extend our knowledge about the Galaxy by adding information that is crucial to better constrain chemodynamical models, revealing the past history of the Milky Way. This Chapter is presented as an already published paper at the Monthly Notices of the Royal Astronomical Society, **?**), which is a sequel of **?**).

MNRAS 000, 1–22 (2017) Preprint 6 February 2018 Compiled using MNRAS LATEX style file v3.0

StarHorse: A Bayesian tool for determining stellar masses, ages, distances, and extinctions for field stars

A. B. A. Queiroz[1,2]⋆, F. Anders[3,2], B. X. Santiago[1,2], C. Chiappini[3,2], M. Steinmetz[3], M. Dal Ponte[1,2], K. G. Stassun[4], L. N. da Costa[2,5], M. A. G. Maia[2,5], J. Crestani[1,2], T. C. Beers[6], J. G. Fernández-Trincado[7,8], D. A. García-Hernández[9], A. Roman-Lopes[10], O. Zamora[9]

[1]*Instituto de Física, Universidade Federal do Rio Grande do Sul, Caixa Postal 15051,Porto Alegre, RS - 91501-970, Brazil*
[2]*Laboratório Interinstitucional de e-Astronomia, - LIneA, Rua Gal. José Cristino 77, Rio de Janeiro, RJ - 20921-400, Brazil*
[3]*Leibniz-Institut für Astrophysik Potsdam (AIP), An der Sternwarte 16, 14482 Potsdam, Germany*
[4]*Vanderbilt University, Department of Physics & Astronomy, VU Station B 1807, Nashville, TN 37235*
[5]*Observatório Nacional, Rua Gal. José Cristino 77, Rio de Janeiro, RJ - 20921-400, Brazil*
[6]*Department of Physics and JINA Center for the Evolution of the Elements, University of Notre Dame, Notre Dame, IN 46556, USA*
[7]*Departamento de Astronomía, Universidad de Concepción, Casilla 160-C, Concepción, Chile*
[8]*Institut Utinam, CNRS UMR6213, Univ. Bourgogne Franche-Comté, OSU THETA, Observatoire de Besançon, BP 1615, 25010 Besançon Cedex, France*
[9]*Instituto de Astrofísica de Canarias, 38205 La Laguna, Tenerife, Spain*
[10]*Departamento de Física, Facultad de Ciencias, Universidad de La Serena, Cisternas 1200, La Serena, Chile*

Accepted XXX. Received YYY; in original form ZZZ

ABSTRACT

Understanding the formation and evolution of our Galaxy requires accurate distances, ages and chemistry for large populations of field stars. Here we present several updates to our spectro-photometric distance code, that can now also be used to estimate ages, masses, and extinctions for individual stars. Given a set of measured spectro-photometric parameters, we calculate the posterior probability distribution over a given grid of stellar evolutionary models, using flexible Galactic stellar-population priors. The code (called StarHorse) can acommodate different observational datasets, prior options, partially missing data, and the inclusion of parallax information into the estimated probabilities. We validate the code using a variety of simulated stars as well as real stars with parameters determined from asteroseismology, eclipsing binaries, and isochrone fits to star clusters. Our main goal in this validation process is to test the applicability of the code to field stars with known *Gaia*-like parallaxes. The typical internal precision (obtained from realistic simulations of an APOGEE+*Gaia*-like sample) are ≃ 8% in distance, ≃ 20% in age,≃ 6% in mass, and ≃ 0.04 mag in A_V. The median external precision (derived from comparisons with earlier work for real stars) varies with the sample used, but lies in the range of ≃ [0, 2]% for distances, ≃ [12, 31]% for ages, ≃ [4, 12]% for masses, and ≃ 0.07 mag for A_V. We provide StarHorse distances and extinctions for the APOGEE DR14, RAVE DR5, GES DR3 and GALAH DR1 catalogues.

Key words: Stars: distances – fundamental parameters – statistics; Galaxy: stellar content

1 INTRODUCTION

Improving the accuracy and precision of stellar distances and ages, as well as individual interstellar extinction measurements, is one of the major tasks of stellar astrophysics in the *Gaia* era. Although the parallaxes from the first data

⋆ E-mail: anna.queiroz@ufrgs.br

release of the *Gaia* mission (Gaia Collaboration et al. 2016)[1] provide a major improvement for stars in the solar vicinity ($d \lesssim 200$ pc), they do not yet reach the precision of spectro-photometric methods for the much larger distances probed by spectroscopic stellar surveys. Even after the final *Gaia* data release, foreseen for 2022, spectro-photometry will provide more precise distances for stars beyond 10 kpc.

A large amount of spectroscopic data for individual stars has become available in recent years from dedicated surveys such as the Sloan Extension for Galactic Understanding and Exploration (SEGUE, Yanny et al. 2009), the Apache Point Observatory Galactic Evolution Experiment (APOGEE, Majewski et al. 2017), the RAdial Velocity Experiment (RAVE; Steinmetz et al. 2006), the Galactic Archaeology with HERMES survey (GALAH; Martell et al. 2017), the LAMOST Experiment for Galactic Understanding and Exploration (LEGUE, Deng et al. 2012), and the Gaia ESO Survey (GES; Gilmore 2012). The combination of such datasets with broad-band photometric data and the astrometric solutions from *Gaia* allow for a much more detailed modelling of the chemo-dynamical history of the Milky Way. On the one hand, *Gaia*'s proper motions and parallaxes, complemented with radial-velocity measurements, enable us to measure stellar phase-space distribution functions with unprecedented precision over a Galactic volume of $\sim 8000\mathrm{kpc}^3$. *Gaia*'s parallaxes (in combination with spectroscopy) also help to estimate stellar masses and ages. And for more distant populations, more accurate spectro-photometric distances can be achieved by improved calibrations in the *Gaia* volume. Such distance estimates are indispensable for mapping the chemical and kinematical properties of Galactic populations using large stellar surveys (e.g., Boeche et al. 2013, 2014; Anders et al. 2014; Recio-Blanco et al. 2014; Nidever et al. 2014; Mikolaitis et al. 2014; Hayden et al. 2015; Carlin et al. 2015; Bovy et al. 2016). If stellar ages are available as well, they can be used to probe the chemo-dynamical evolution of different Galactic components much more directly (e.g., Zoccali et al. 2003; Haywood et al. 2013; Mitschang et al. 2014; Anders et al. 2017; Mackereth et al. 2017).

In Santiago et al. (2016), we presented a Bayesian inference code to determine spectro-photometric distances for large survey samples, both in the optical and near-infrared (NIR). Since then, our group has extended that algorithm in several ways, improving the code's flexibility for different input data, updating priors and likelihood functions, and adding extinction, ages, and masses as parameters to be inferred by the method. In this paper we demonstrate these new capabilities. The paper is structured as follows: In Sec. 2 we describe our method to estimate stellar parameters, distances, and extinctions. Section 3 presents the recent updates to our code. We provide an analysis of the performance of our code in terms of internal accuracy and precision in Sec. 4, using simulated stars, focussing especially on the new parameters mass, age, and extinction. We also discuss how biased spectroscopic parameters influence the estimated quantities. In Sec. 5 we compare our distances to several previous mass, age, and distance determinations that can be used as a reference. In Sec. 6 we describe a `StarHorse` application to a few spectroscopic surveys, with the purpose of delivering public releases of distances and extinction, We refrain from releasing ages and masses for the time being since their accuracy is still dependent on availability of Gaia-DR1 parallaxes and additional improvements. Gaia-DR2 will certainly improve their application to large volumes and datasets. We conclude the paper with a summary and future plans in Sec. 7.

[1] http://sci.esa.int/gaia/

2 THE METHOD

Our method uses a set of spectroscopically-measured stellar parameters (typically effective temperature, $T_{\rm eff}$, surface gravity, $\log g$, and overall metallicity [M/H]), photometric magnitudes, m_λ, and parallax, π, to estimate the mass, m_*, age, τ, distance, d, and extinction (in V band, A_V) for individual stars. The measured quantities are compared to predictions from stellar evolutionary models, following a statistical approach that is similar to previous works (e.g., Burnett & Binney 2010; Burnett et al. 2011; Binney et al. 2014), and that generalises the method presented in Santiago et al. (2016).

The calculations rely on three important assumptions: Most importantly, we assume that the stellar models are correct, which might not be true for metal-poor stars as well as other limitations in the current stellar models, i.e., that the object of interest follows a canonical single-star evolutionary track. We caution that this assumption, even if a star is apparently single, can be violated to various degrees in practice, leading first and foremost to incorrect stellar mass and/or age estimates (e.g., Brogaard et al. 2016; Yong et al. 2016; Fuhrmann & Chini 2017; Lagarde et al. 2017). The second assumption is that the observational uncertainties of the measured parameters follow a normal distribution. The third assumption is that the observed measurements are independent, a condition that can also be violated in practice.

We can then calculate the probability that a set of independent measured parameters $\vec{x} = \{x_1, ..., x_n\}$ with associated Gaussian uncertainties $\vec{\sigma_x}$ is drawn from a set of theoretical values $\vec{x_0}$, predicted by some model $\mathcal{M}$, by writing:

$$P(\vec{x}, \vec{\sigma_x}|\vec{x_0}) = \prod_i \frac{1}{\sqrt{2\pi}\ \sigma_{x_i}} \exp\left[-\frac{(x_i - x_{0_i})^2}{2\sigma_{x_i}^2}\right]. \quad (1)$$

The above expression is called the likelihood of measuring the set $\{\vec{x}, \vec{\sigma_x}\}$ given a model $\mathcal{M}(\vec{x_0}[\vec{\theta}])$. Using Bayes's theorem, we now compute the posterior probability distribution (the probability of the model, given the data) as:

$$P(\vec{x_0}|\vec{x}, \vec{\sigma_x}) = \frac{P(\vec{x}, \vec{\sigma_x}|\vec{x_0})\ P(\vec{x_0})}{P(\vec{x}, \vec{\sigma_x})}. \quad (2)$$

The numerator contains the likelihood and the model priors $P(\vec{x_0})$, and the denominator is the marginalized likelihood. It depends only on the measured parameters, being a constant through all the models that can be normalised out.

In our case, the model family $\mathcal{M}(\vec{\theta})$ consists of a grid of stellar models computed for different ages, metallicities, and initial masses, convolved with a grid of distances and extinctions (modifying the apparent magnitudes of each stellar model). To evaluate the probability of some specific model quantity, ϑ (usually one that cannot be measured directly),

we now compute the marginal posterior probability distribution function (PDF) for this quantity, by integrating over all variables of Equation (2), except ϑ:

$$p(\vartheta) \coloneqq P(\vartheta|\vec{x},\vec{\sigma_x}) = \int \mathrm{d}x_{0,0} \ldots \mathrm{d}x_{0,n} P(\vec{x_0}[\vec{\theta}]|\vec{x},\vec{\sigma_x}). \quad (3)$$

As mentioned earlier, a typical set of measured parameters includes $\vec{x} = \{[\mathrm{M/H}], T_{\mathrm{eff}}, \log g, m_\lambda, \pi\}$, or any subset of these. The model parameters ϑ we compute are mass, m_*, age, τ, distance, d, and V-band extinction, A_V. Our code delivers various statistics for the desired quantities. As in Rodrigues et al. (2014) and Santiago et al. (2016), for each quantity we compute the median of the marginalised posterior probability distribution, $p(\vartheta)$ (Eq. 3), along with its 5%, 16%, 84% and 95% percentiles.

3 CODE UPDATES

In this section, we explain the technical details of our code in more detail (for an overview see the flow diagram in Fig. 1). We encourage the reader to contact the developers[2] [3] for any questions or further details about the code. Via a parameter file, the user can choose the set of stellar models to be used, the available photometric and spectroscopic data, the treatment of extinction (whether to correct photometry for reddening or whether to include extinction as a parameter to be estimated), and the set of priors, among other options. Once the evolutionary models and the data are read in, the code operates according to the options chosen in the parameter file. These options, along with the other updates since Santiago et al. (2016), are detailed in the next subsections. Readers interested only in the overall performance of the code may skip these.

3.1 Including Parallax as a measured parameter

To adapt our method to the new era of astrometric surveys like *Gaia*, JASMINE (Gouda 2012), VLBA (Melis et al. 2014), and SKA (Imai et al. 2016), we introduced parallax as an optional measured input parameter for our code. As explained in the previous section, the likelihood can be extended for a generic group of measured parameters, so the method presents no difficulties to introduce the parallax in the likelihood, and it allows for much more precise estimates of stellar masses, ages, and extinction. When the user decides to use parallaxes as the primary input, we fix the range of distances for all models to be consistent with that measurement within 3σ (see §3.2.1 below). If this is not specified, the possible range of distances to be probed for each stellar model is derived by matching an observed apparent magnitude, m_λ (within $\pm 3\sigma_{m\lambda}$), in some filter to the corresponding model absolute magnitude.

3.2 Stellar parameters posterior

Currently our code can determine distances, ages, masses, and extinctions, given a set of measured parameters by marginalising the joint posterior PDF. Below we explain in more detail how we build the values of distance, extinction, ages, and masses covered by the PDF.

3.2.1 Distance

If no reliable parallaxes are available, or if they are only available for a subset of stars, the range of distances to be probed comes from the available measured apparent magnitudes. We choose a master filter, λ, and create an array of length N_d that ranges from $m_{\lambda 0} \pm 3\sigma_{m,\lambda 0}$, where $m_{\lambda 0}$ stands for intrinsic measured apparent magnitudes in the master filter. For each value of this array we compute the distance modulus, $(m_{\lambda 0} - M_\lambda)$, for the absolute magnitudes in the model grid; these values are then finally transformed into an array of possible distances, d. When A_V is not being estimated together with distance, the code assumes that the given magnitudes are previously corrected by the known extinction. See Section 3.2.2 for details of the estimation of A_V. As explained in §3.1, if the user decides to use parallax measurements as the primary input, we build the distance array by inverting the array of allowed parallaxes. We then transform d to intrinsic distance moduli that do not depend on colour or extinction. The d and $(m - M)$ values are then used in the priors and likelihood to build the posterior PDF.

3.2.2 Extinction

When multi-band photometry over a sufficient wavelength range is available, one can use the measured colours of a star to estimate interstellar dust extinction. When the intrinsic magnitudes are constrained by spectroscopic measurements, this extinction measurement can become very precise (e.g., Rodrigues et al. 2014). Our code can now also be used to determine extinction towards stars, by adding another free dimension to the model space.

When parallaxes are not available, we build a distance moduli that comes from the apparent magnitude $(m_\lambda - M_\lambda)$, as explained in §3.2.1, but now the measured magnitudes are assumed not to be intrinsic. The distance moduli must then be corrected by an a priori unknown extinction: $(m_{\lambda 0} - M_\lambda) = (m_\lambda - M_\lambda) - A_\lambda$. For each stellar model and each possible distance modulus, $(m_\lambda - M_\lambda)$, we thus create N_{A_V} random A_V values from a previously defined range of possible A_V. If there is no initial guess of the A_V for the given star, this range of A_V values is kept fixed as $[-0.1, 3.0]$. If some expectation for A_V is available (an A_V prior, $A_{V,0}$), we probe extinction in the range $[A_{V,0}/3, 3 \cdot A_{V,0}]$. We then transform the A_V to A_λ values using a chosen extinction curve (Schlafly et al. 2016 by default; see Sect. 3.4 for a discussion, and subtract it from $(m_\lambda - M_\lambda)$. Since the model space is large, we usually use $N_{A_V} = 3$ to lower the computational cost. As long as the spectroscopic measurements do not confine the solution to a very small volume in model space, the marginalised PDFs over extinction and distance remain well-sampled.

When parallax information is available, the dereddened distance modulus array, $(m-M)_0$, is determined directly from the parallax. To determine the extinction we then use the reddened distance modulus arrays built from the apparent magnitudes, $(m_\lambda - M_\lambda)$, and the difference between those two naturally delivers A_λ.

[2] Anna Barbara Queiroz, Email: anna.queiroz@ufrgs.br
[3] Friedrich Anders, Email: fanders@aip.de

3.2.3 *Masses and Ages*

Because masses and ages are quantities provided by the grid of evolutionary models, they are simply repeated over the additional dimensions of distance and extinction. Therefore, once we have a PDF from equation (3), we can directly estimate these parameters by marginalising over the distance and extinction dimensions.

3.3 New spatial, chemical, and age priors

Our code uses several priors that summarise our prior knowledge about the initial mass function and the stellar population structure of the Milky Way, including the thin and the thick disk, and the stellar halo. For each Galactic component, these priors include the spatial density distribution, a metallicity distribution function (MDF) and an age distribution. In Santiago et al. (2016), we adopted the same priors as Binney et al. (2014). In the current version, we updated our default structural parameters (solar position, scale lengths, scale heights, normalisations) from Binney et al. (2014) to Bland-Hawthorn & Gerhard (2016).

Since APOGEE and other surveys are now probing also the inner regions of the Milky Way, we have also added simple spatial priors for the bulge/bar. The simplest choice of bulge spatial prior is a spherical exponential model with a exponential e-folding length of $0.5 - 1.0$ kpc. We also added the oblate model described by Dehnen & Binney (1998). Finally, as our default model we included a bar-like bulge model from Robin et al. (2012). Their models assume the bulge to be a triaxial ellipsoid, either boxy or disky (or yet a combination of both depending on the plane of projection), and with density laws that can be a $sech^2$, an exponential, or a Gaussian. Our code has been tested with one- and two-component model priors. Our default model is the S ellipsoid (bar component) taken from the "S+E" case listed in Table 2 of Robin et al. (2012). This "S+E" model was the minimum likelihood one among the models presented by the authors. The E component was removed based on the revision of the thick-disk structure and its extrapolation towards the inner Galactic regions made by Robin et al. (2014), which effectively rendered the classical ellipsoid bulge unnecessary. We refer the interested reader to Robin et al. (2012) and Robin et al. (2014) for more details.

Fig. 2 shows the contributions of each Galactic component spatial distribution as a function of distance, for four representative directions. In the upper left panel we show a direction towards the inner Galaxy $(l, b) = (20, 8)$; in this case the bar/bulge component is the dominant population at heliocentric distances of ~ 6 kpc, its density decreases rapidly toward greater distances. The upper right panel shows a direction toward the same Galactic longitude, but at higher latitude. In this case the we miss the bulge, and notice that each of the other components dominates at a certain distance range.The lower panels shows directions away from the Galactic centre. In the lower left panel $(l, b) = (90, 30)$, we see that the contribution for the disks dominates out to 3.5 kpc, in the lower right panel $(l, b) = (150, 60)$ the halo dominates already for $d > 2$ kpc.

Our new age and metallicity priors for the four Galactic components are all assumed to be Gaussians. The corresponding mean and standard deviation values for each case are provided in Table 1. The motivation for this change is twofold: 1 - simplicity: they are simple functions, easily computed, which makes them ideal for the computationally intensive parameter estimate process used here; 2 - they are made broad enough to accommodate most or all of the recent age and metallicity distributions found in the literature, which are not only diverse, but also often conflicting. We assume that the impact of this choice is minor, though we are aware that the age and mettalicity distribution are not necessarly gaussians, by taking this approach, we avoid making our priors too specific, but do not completely overlook the knowledge accumulated about the different Galactic components.

Table 1. Adopted parameters of the Gaussian age and metallicity priors for the Galactic components.

Component	Mean age	σ age	Mean [M/H]	σ[M/H]
Thin disk	5.0 Gyr	4.0 Gyr	-0.2	0.3 dex
Thick disk	10.5 Gyr	2.0 Gyr	-0.6	0.5 dex
Halo	12.5 Gyr	1.0 Gyr	-1.6	0.5 dex
Bulge	10.0 Gyr	3.0 Gyr	0.0	0.5 dex

We note that the previous age priors from Santiago et al. (2016) assigned zero probability to disk stars older than 10 Gyrs and to thick disk or halo stars younger than this value. Recent results found in the literature pose a challenge to such simple age step functions. One example is the discovery of young α-enhanced stars, likely thick-disk members (Chiappini et al. 2015). The previous metalicity priors were also narrower, specially for the thin-disk, essentially ruling out any thin disk star more metal-poor than $[Fe/H] \simeq -0.6$. The changes made to these components also make them more in sync with our current understanding of the bulge populations, for which there is also recent evidence for a larger fraction of stars younger than $\simeq 5$ Gyrs (Bensby et al. 2013; Valle et al. 2015).

3.4 A new default extinction curve

The adopted extinction curve, i.e. the dependence of the absolute extinction on wavelength, has of course an influence on the distances and extinctions provided by our code.

To quantify this effect, we recently implemented the one-parameter extinction curve presented by Schlafly et al. (2016), derived from APOGEE spectroscopy in combination with Pan-STARRS1, 2MASS, and WISE data, as an alternative to the Cardelli et al. (1989) curve that was determined based on very few stars. For the mostly low-latitude APOGEE DR14 sample, where the sensitivity of our results to the chosen extinction law is arguably highest, we tested the effect of changing the extinction curve from Cardelli et al. (1989) to Schlafly et al. (2016).

Our tests showed that, if both optical (APASS) and near-infrared magnitudes are available (i.e. for the brighter stars), the systematic effect of the adopted extinction curve is almost negligible: median differences in the inferred parameters range in the 1%-percent regime, although there are some weak systematic trends with age. The main differences in the inferred parameters arise when only 2MASS magnitudes are available: in this case the results

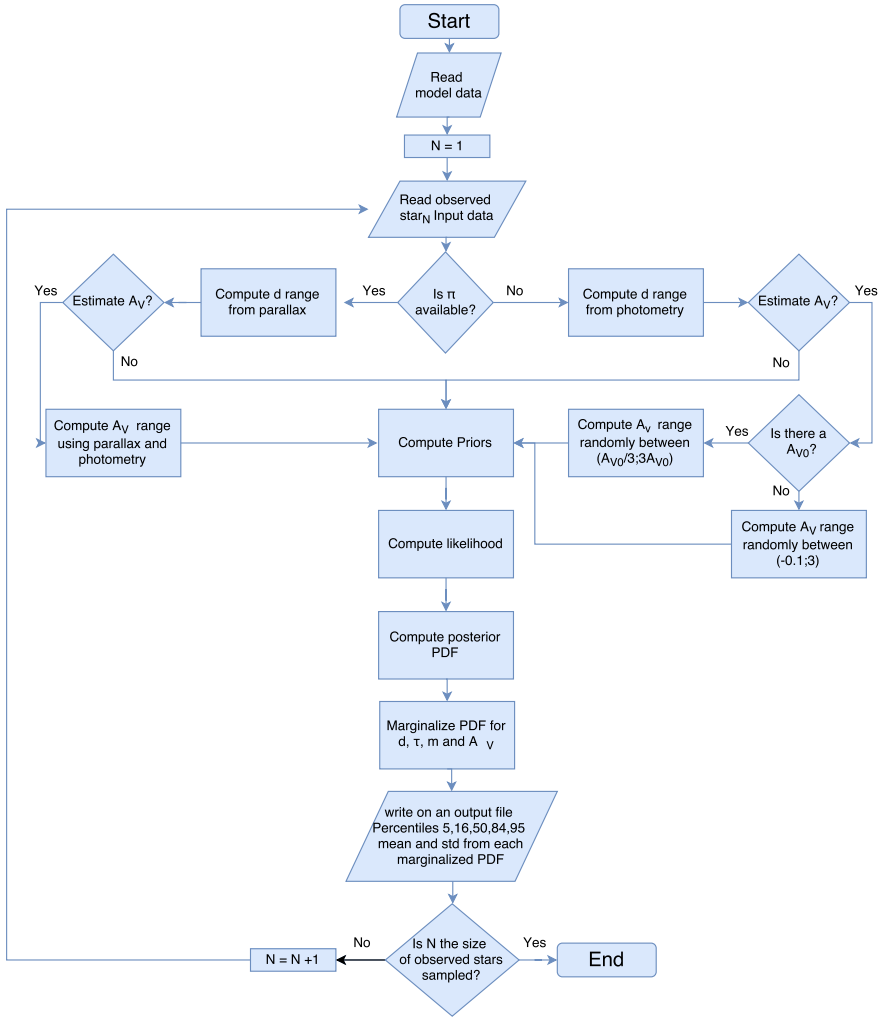

Figure 1. `StarHorse` flux diagram. See Sec. 2 and 3 for details.

using Schlafly et al. (2016) yield ∼ 5% lower A_V, ∼ 9% greater ages, ∼ 0.6% greater distances, and ∼ 11% higher A_V. Since the Schlafly et al. (2016) extinction curve is much more realistic, and its adoption also slightly improves the convergence of the code for high-extinction stars (i.e. distances to ∼ 10,000 more APOGEE DR14 stars could found), the default `StarHorse` extinction curve is now Schlafly et al. (2016).

4 TESTS WITH SIMULATED STARS

To validate our code, we carried out several tests using simulated stars. Since one of our main goals is to apply `StarHorse` to field stars with reliable parallaxes to infer masses and ages, we include parallax in the set of observed quantities of our simulated stars, and use them to constrain our distance range.

The first sample of simulated stars we used is identical with the set used in Santiago et al. (2016), except for the dis-

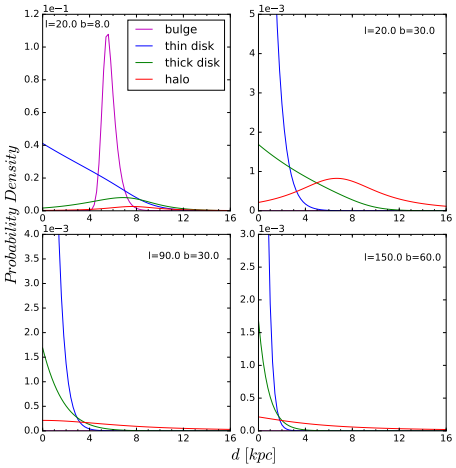

Figure 2. Spatial profile for the Galactic components used in the StarHorse priors. Each panel shows the behaviour of the prior probability density with distance for a given direction in Galactic coordinates (l, b).

tance range and the assumed spectroscopic uncertainties. It consists of 5000 randomly drawn PARSEC models (Bressan et al. 2012), convolved with Gaussian errors in the spectrophotometric parameters and parallaxes (see details in Table 3). The error values for the "high-res" version of this simulation were inspired by the spectroscopic uncertainties from the APOGEE DR14 results, while the low-res case was based on typical uncertainties from the SEGUE and RAVE surveys. In both cases the samples contain stars with distances between 0.05 and 1 kpc (typical *Gaia*-TGAS distances), random galactic positons, and extinctions from Schlegel et al. (1998).

The PARSEC simulated stars are useful to map the internal accuracy and precision of our estimated distances, ages, masses, and extinctions over a wide input parameter range. The caveat is that the PARSEC sample sets are not representative of a real magnitude-limited sample of stars in our Galaxy. By randomly picking PARSEC models, we tend to oversample young stars, regardless of metallicity, relative to most survey data in the nearby Galaxy. This also means that our prior knowledge about Galactic stellar populations does not apply to these simulations, so that in this case we set all priors to unity.

To test the code in more realistic scenario, we also use a TRILEGAL (Girardi et al. 2012) population-synthesis simulation of an APOGEE-TGAS-like sample of giant stars. The details of this simulation are given in Table 2; we describe the main features briefly here. The underlying stellar models of TRILEGAL are from Marigo et al. (2008), which are similar but not identical to our default PARSEC 1.2S models. We used a Chabrier (2003) log-normal initial mass function (IMF) for all Galactic components (thin disk, thick disk, bulge, and stellar halo), and the default spatial distribution, density normalization, star-formation rate (SFR), and age-metallicity relation (AMR) for all components (see Table 2). Extinction was assumed to result from an exponential dust disk with calibration at infinity of $A_V = 0.0378$ mag for the Galactic poles, and the photometry is in the *UBVRIJHK* system (Maíz Apellániz 2006). The Solar position and Solar height above the disk were assumed to be $R_\odot = 8.7$ kpc and $Z_\odot = 24.2$ pc, respectively (deviant from the values of our Galactic priors, $R_\odot = 8.2$ kpc and $Z_\odot = 11.1$ pc; see Sec. 3.3). To simulate APOGEE-TGAS-like observations, we convolved the TRILEGAL stellar parameters with Gaussian errors, as in the PARSEC (*high-res*) sample, and introduced cuts in $\log g$ and distance. The uncertainty values and stellar parameter ranges for TRILEGAL sample are again listed in Table 3.

The main aim of using this TRILEGAL simulation was to test the impact of the different Galactic priors in our parameter estimates. Therefore, we ran StarHorse on the TRILEGAL sample for three prior configurations: i) no spatial, age, and metallicity priors, only the IMF; ii) IMF and spatial priors only; iii) all priors.

4.1 Internal accuracy and precision

Figure 3 shows the results of our PARSEC simulated-star tests (high-res case). The first two rows show the relative errors in distance, $(d_{SH} - d_{True})/d_{True}$, where d_{SH} are the distances estimated by our code (SH standing for StarHorse). Each panel shows these same errors as a function of a different parameter. The last panels on the right show the relative distance errors (top row) and uncertainties (2nd row) mapped onto the $\log g$ *vs.* $T_{\rm eff}$ diagram. The first line of Table 4 shows the relative distance error values that correspond to the 5% -ile, 16% -ile, 50% -ile, 84% -ile, and 95%-ile positions of the relative error distribution, when their signs are omitted. We also list the median value of the full error distribution, to quantify the presence of systematic trends. For example, we see that 50% of the simulated stars have distance errors of less than 6%, and 84% have distance errors below 16%. There is no strong systematic trend with any of the parameters, apart from an increase in the errors for larger distances and for lower $\log g$ values (giants). We also note that the discreteness of the PARSEC model grid used is visible in most of the panels.

The remaining rows of Fig. 3 shows the same type of plots, but now with the relative errors in age, mass, and A_V. As before, the percentiles of the relative error distributions are listed in Table 4. As in the case of distances, the mass estimates (rows 5 and 6 in Figure 3) do not suffer from any clear systematics with the main parameters, apart from the trend of increasing errors with distance. There is a subset of mostly subgiant and dwarf stars ($\log g > 3.5$, and $m_{ast} < 0.8 m_\odot$) with very-well determined masses. From Table 4, we see that 50% (84%) of the estimated masses agree with the true values within 7 (22)%, and that the outliers are predominantly young (massive) evolved stars, which are rare in the Milky Way field.

As for ages, shown in the 3rd and 4th rows of Figure 3, catastrophic errors, of 100% or more, occur for about 15% of the stars. These stars are not restricted to a small subset of parameter space. But age is the main parameter leading to these catastrophic errors, which are more frequent for $\tau < 1$

Table 2. Adopted geometry, local or central calibration and SFR+AMR for the Galactic components simulated with TRILEGAL

Component	Spatial distribution	Local/Central Calibration	SFR+AMR
Thin disk	Squared hyperbolic secant Girardi et al. (2005)	Local 55.40 $M_{\odot}pc^{-2}$	2-step age + Fuhrmann (1998) + α-enh Girardi et al. (2005)
Thick disk	Squared hyperbolic secant Girardi et al. (2005)	Local 0.001 $M_{\odot}pc^{-3}$	11-12 Gyr const. + Z = 0.008 with $\delta[M/H] = 0.1$dex
Halo	Power law de Jong et al. (2009)	Local 0.0001 $M_{\odot}pc^{-3}$	12-13 Gyr + Ryan et al. (1996) $[M/H]$ distribution
Bulge	Triaxial bulge Vanhollebeke et al. (2009)	Central 406 $M_{\odot}pc^{-3}$	10 Gyr + Zoccali et al. (2003) $[M/H]$ + 0.3 dex

Table 3. Summary of the reference data: parameter ranges, uncertainties, and provenance.

Sample	$\sigma(\pi)$ [mas]	d range [kpc]	$\sigma(T_{\rm eff})$ [K]	$T_{\rm eff}$ range [K]	$\sigma \log g$	$\log g$ range	σ [M/H]	[M/H] range	σ mag	mag range [V mag]	filters
PARSEC high-res	0.3	0.05 – 1	70.0	3000 – 7000	0.08	1 – 5	0.03	−2.5 – 0.5	0.025	−2 – 24	$BVgriJHK_s$
PARSEC low-res	0.3	0.05 – 1	95.0	3000 – 7000	0.24	1 – 5	0.12	−2.5 – 0.5	0.025	−2 – 24	$BVgriJHK_s$
TRILEGAL	0.3	0.05 – 1	70.0	3000 – 7000	0.08	1 – 4.1	0.03	−2.5 – 0.5	0.025	4 – 13	$BVRIJHK_s$
Detached Eclipsing Binaries	0.04	0.01 – 65	80	4320 – 5730	0.02	1 – 3.6	0.12	−1.1 – 0.1	0.03	0.7 – 18	$BVRI$
Other Eclipsing Binaries	0.36	0.03 – 1	256.0	3880 – 30300	0.02	2.9 – 4.5	0.1	0.03 – 0.2	0.06	5 – 12	$BVRIJHK_s$
CoRoGEE stars	0.007	0.8 – 10	90.0	4000 – 5500	0.05	1.4 – 3.0	0.03	−2.5 – 0.5	0.025	11 – 16	$BVgriJHK_s$
OCCASO clusters stars	0.06	0.05 – 6	60.0	4300 – 5300	0.1	1.7 – 3.2	0.2	0.0 – 0.4	0.03	8 – 15	JHK_s

Gyr. There is also some dependence on distance (i.e., low parallaxes, for which the parallax error is relatively large) and mass (or $\log g$). Since dwarfs change their position in the spectroscopic Hertzsprung-Russell diagram only slightly on long timescales, ages for dwarfs are more uncertain; the age PDF will tend to be very flat. The A_V errors shown in the last two rows are within 0.05 (0.1) mag for 50% (84%) of the stars, with no clear systematic effects.

Figure 4 shows the results of our TRILEGAL test sample, in the same style as Fig. 3, for the case where all priors (IMF, spatial, age, and metallicity) are used. Although the stellar-parameter range of the TRILEGAL sample is similar to the PARSEC simulations, the resulting error distributions vary considerably when compared to the PARSEC results. There is a relative scarcity of low-mass and young stars in the TRILEGAL simulations when compared to PARSEC. Most dwarfs are removed by the APOGEE colour cut, and most red M dwarfs ($m_* < 0.8 m_{\odot}$, $\log g > 4$) are too faint to be seen. Likewise, most stars, even in the thin-disk component, are older than $\tau \simeq 500$ Myr. Relatively fast evolutionary stages, like post-HB phases, are also less frequent in the TRILEGAL simulations.

The first two rows of Figure 4 show that there is a small trend towards underestimating distances overall, especially for hot dwarfs and subgiants (high $T_{\rm eff}$ and $\log g$ clouds in the upper row). Errors in all four parameters also tend to systematically increase with distance. Slight general trends are also observed in the sense of overestimating ages, and underestimating masses and extinction (these latter two parameters seem to be more affected for low $T_{\rm eff}$ stars). Still, typical errors are of order $\simeq 8\%$, $\simeq 19\%$, $\simeq 6\%$, and $\simeq 0.04$ mag, respectively, for distances, ages, masses and A_V (Table 4). We also notice that the absence of a large number of young main sequence stars significantly reduces the occurrence of catastrophic age errors in TRILEGAL.

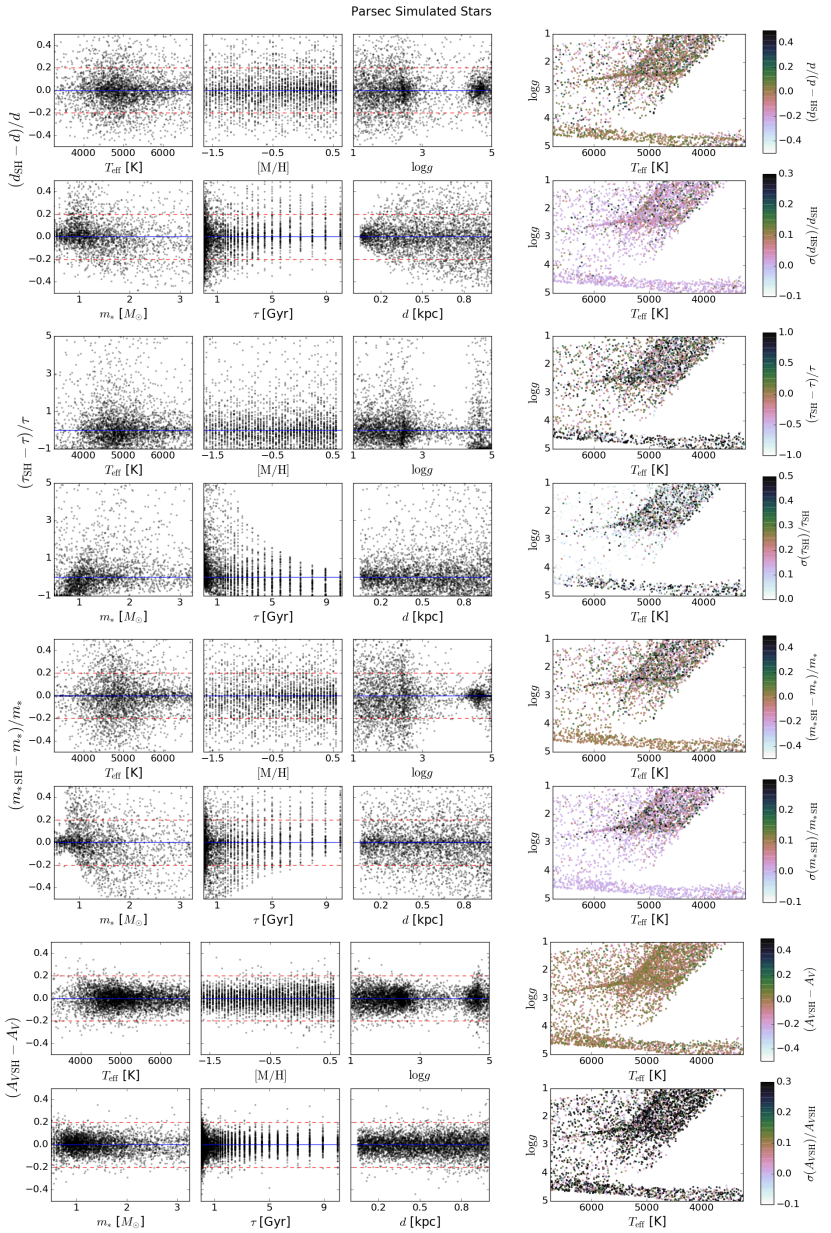

Figure 3. `StarHorse` relative errors for the PARSEC high-res simulations. For each parameter, the six panels on the left show the relative errors, d (top rows), τ (third and fourth row), m_* (fifth and sixth row), A_V (last rows) as a function of the true parameters. The solid blue line is the identity line, and the dashed red lines correspond to ±20% errors (except for ages: 40%). The panels on the right show the relative errors (top panel) and uncertainties (bottom panel) in the $\log g$ vs. $T_{\rm eff}$ plane.

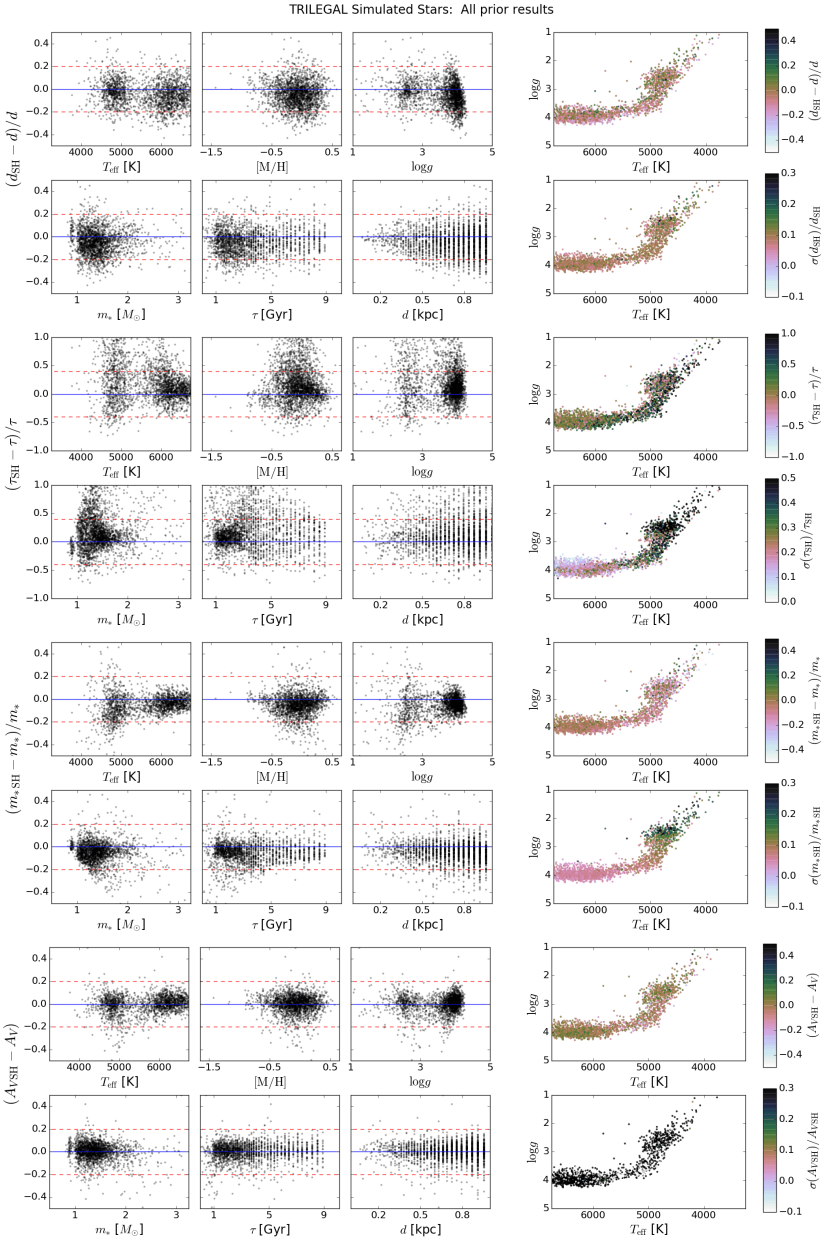

Figure 4. Relative distance, age, mass, and V-band extinction errors for the TRILEGAL simulations, in the same style as Fig. 3.

To test the influence of our prior knowledge, the TRILEGAL results shown in Fig. 4 (all priors included) can be compared to Fig. A2 in Appendix A. That figure shows the corresponding results for the case when no priors were adopted. In general, the results in the *all priors* and in the *no priors* cases are quite similar, indicating that the accuracy of our code is robust to prior assumptions. We also tested the case where only the spatial priors were used, but not the age and MDF ones. As expected for this intermediate case, the panels are again very similar to those shown in Figures 4 and A2.

This is further corroborated by Figure 5, where we show the relative error distributions of age, distance, mass, and A_V for the three combinations of priors, and separated for subgiants/hot dwarfs and giants. The histograms confirm the trends seen in the scatter plots, and they also show that the parameter estimates are not strongly dependent on the priors adopted, at least out to our maximum distance of 1 kpc (TGAS volume). We note that the spatial density profiles, SFH and MDF used by TRILEGAL are not the same as those in `StarHorse`, which shows the importance of adding basic and non-restrictive priors in the parameter inference.

4.2 Effect of systematic stellar parameter errors

As in Santiago et al. (2016), we also tested the effect of systematic offsets in the observed quantities on our results, using the PARSEC samples. The results are shown in Figure 6. Again we split the simulated samples into giants and dwarfs. Each column corresponds to a given parameter for which shifts were applied, keeping the other parameters at their observed (but systematics-free) value. Each panel shows the mean, the median, and the dispersion around the mean values of the relative error (over all stars), as a function of the shift parameter.

In almost all panels, the difference between the mean and median relative errors is very small, attesting to the existence of relatively few outliers. The dispersion around the mean is rarely larger than 20% (or 0.2 mag in the case of extinction) in most cases studied. The exception is the relative age error, for which the mean is much farther from zero than the median, and the dispersion is of order $\simeq 100\%$ in the case of giants, and even larger for dwarfs (see also discussion above). On average, however, the effect of systematic errors on our estimated parameters are typically less than $\pm 10\%$. In the following we discuss some more conspicuous effects.

Systematic errors in $T_{\rm eff}$ affect almost all inferred parameters for both dwarfs and giants. The effect of (under)overestimating temperatures on dwarfs is perhaps simpler to interpret, as it leads to best matching models of (lower)higher masses, therefore (less)more luminous. The apparent distance modulus is correspondingly biassed too (low)high, yielding either (smaller)larger inferred distances or A_V, or a mixture of both. For the giants, evolutionary timescales are shorter, making age a central parameter. In their case, an (under)overestimated $T_{\rm eff}$ requires a (older)younger (and therefore (less)more massive and luminous) progenitor, and leads to concordance models of higher apparent distance moduli.

The systematic effects of metallicity biases on the inferred parameters are of lower amplitude as compared to $T_{\rm eff}$. This is consistent with $T_{\rm eff}$ having a tighter correlation with the photometric parameters, and hence more strongly affecting the likelihood functions. Estimated masses are affected when the metallicity is biased. An (over)underestimated metallicity leads to a better match of a given star to models of (higher)lower metallicity, which will be of (higher)lower mass for a fixed luminosity (i.e., fixed apparent magnitudes and distance). For giants, the higher(lower) masses will again require younger(older) progenitors.

The case of $\log g$ is such that it affects distances more strongly. This has been investigated before by Santiago et al. (2016), with similar results. An (under)overestimate in *logg* leads to an (over)underestimate in the distances, since the data for a star become more consistent with models of stars (more)less luminous than it actually is.

Parallaxes (last column of Figure 6) also predominantly affect distances, in the expected sense. A slight effect on masses and ages of giants can also be seen, since an (under)overestimated parallax will require (more)less luminous giants, therefore shifting the models towards (younger)older ages with (higher)lower mass progenitors.

5 EXTERNAL VALIDATION

Up to this point, we have shown `StarHorse` results for simulated stars, for which we previously know all their stellar parameters. Although TRILEGAL delivers realistic star-counts simulations for the Galaxy, real data can present different behaviour from the assumptions we made on the simulations. In this section we test `StarHorse` results for observed data. We choose samples of stars from eclipsing binaries, asteroseismology, and open clusters. Another important difference with respect to the validation carried out in the previous section is that here we will compare our estimated distances, ages, masses, and extinction values out to distances larger than 1 kpc.

5.1 Eclipsing Binaries

In this section we show `StarHorse` validations with samples of Eclipsing Binaries (EBs). EBs can give precise stellar masses and radii, which in turn yield precise surface gravities. If temperature is also available, these stars can provide a good benchmark for estimating distances, ages, masses, and extinctions. Here we show tests on two samples: one is made up of detached binary systems with individual values of stellar parameters, the other has EBs that are photometricaly unresolved.

5.1.1 Detached Eclipsing Binaries

We use the sample of EBs from Ghezzi & Johnson (2015) as a first comparison sample to our `StarHorse` estimates. Those authors carried out a literature search for detached binary systems with at least one evolved star to be used as a benchmark for the determination of masses. This sample contains a total of 26 binaries with photometry, atmospheric parameters, parallaxes, ages, masses, and extinctions. The majority of the sample is composed of stars from the Large and Small Magellanic Clouds (LMC, SMC), but some stars

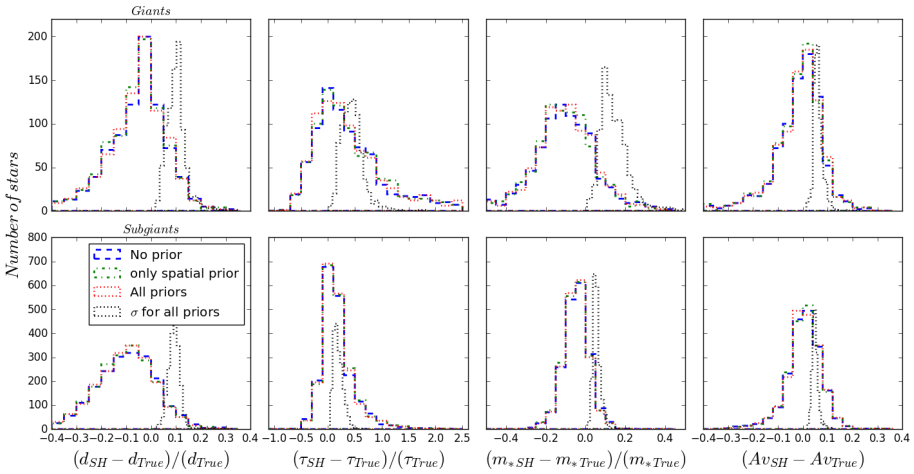

Figure 5. Testing priors with TRILEGAL simulations. The figure shows the distributions of relative errors and uncertainties in distance (leftmost column), age (second column from left), mass (third column from left) and A_V (rightmost column). The top panels show the results for giant stars ($\log g < 3.5$) and the bottom ones are for subgiant stars ($4.1 > \log g > 3.5$). The different lines in each panel correspond to the 3 different prior assumptions used. The blue line represents the results when no spatial, age and metallicity priors are adopted, the green line is based on spatial priors only, and the red line shows the results for all priors. The black lines represent the distribution of StarHorse uncertainties normalised by the parameter, only for the all priors case.

are near the Solar vicinity ($d < 1$ kpc). As we see in Table 3, this sample contains mainly giant and subgiant stars ($\log g < 3.6$) with low metallicity. To run StarHorse we used as input the photometry, $T_{\rm eff}$, [Fe/H], and π given in Table 1 of Ghezzi & Johnson (2015), and $\log g$ given in their Table 2.

StarHorse recovered distances, ages, masses and extinctions for 24 out of 26 stars. Fig. 7 compares these results to the more fundamental determinations of Ghezzi & Johnson (2015). For the distances, shown in the upper left panel of Fig. 7, the reference distance is the inverse of the *Hipparcos* input parallaxes used by those authors. Because the sample includes stars either in the Solar Neighbourhood, ($d < 1$ kpc), as well as stars at LMC/SMC distances, we show these latter as a separate inset in the figure. The agreement is excellent, with only a small degradation for the larger distances to LMC and SMC stars, whose parallax uncertainties are larger (see the panel inset). The mean uncertainty on the parallax of this sample is lower then the simulated samples; see Table 3. This is probably the reason for such a good agreement in distances. In the same figure, we show the comparison between StarHorse and PARAM da Silva et al. (2006) ages (which incorporate results from asteroseismology using a method similar to StarHorse; upper right panel), and the comparison between StarHorse masses and those taken from asteroseismology scaling relations (lower left panel; for the references on the masses, see Table 2 in Ghezzi & Johnson 2015). We also show the comparison between StarHorse A_V and $3.1E(B-V)$ (lower right panel), where the references for E(B-V) are in Table 1 of Ghezzi & Johnson (2015).

From Figure 7, we see that StarHorse yields ages that are systematically larger than those from PARAM. The median age offset is of 22%. Still, most of the StarHorse ages appear to agree with PARAM ages to within 50%. The two age determinations are also consistent with each other for most stars, considering both error bars. Table 4 shows that 50% (84%) of the estimated ages have errors below 25% (76%). As for the masses, the agreement between our estimates and those from asteroseismology are somewhat better. StarHorse masses tend to be smaller by 12%. The error bars and discrepancies relative to PARAM values are relatively smaller as well, with most of stars having errors of 17% or smaller. The extinction estimates also agree well with the ones from the literature, despite the large error bars. Most of the stars have an A_V error below 0.18 mag, with a moderate systematic effect (−0.07 mag). We note that the systematics between StarHorse and the reference sample values cannot be due to systematics in the input atmospheric parameters, since both methods used the same data as input.

5.1.2 *Other Eclipsing Binaries*

As a second comparison with EBs, we use the sample from Stassun & Torres (2016), which contains 156 systems. Their sample is composed of stars with precise stellar radii and effective temperatures. Most of the stars have also avail-

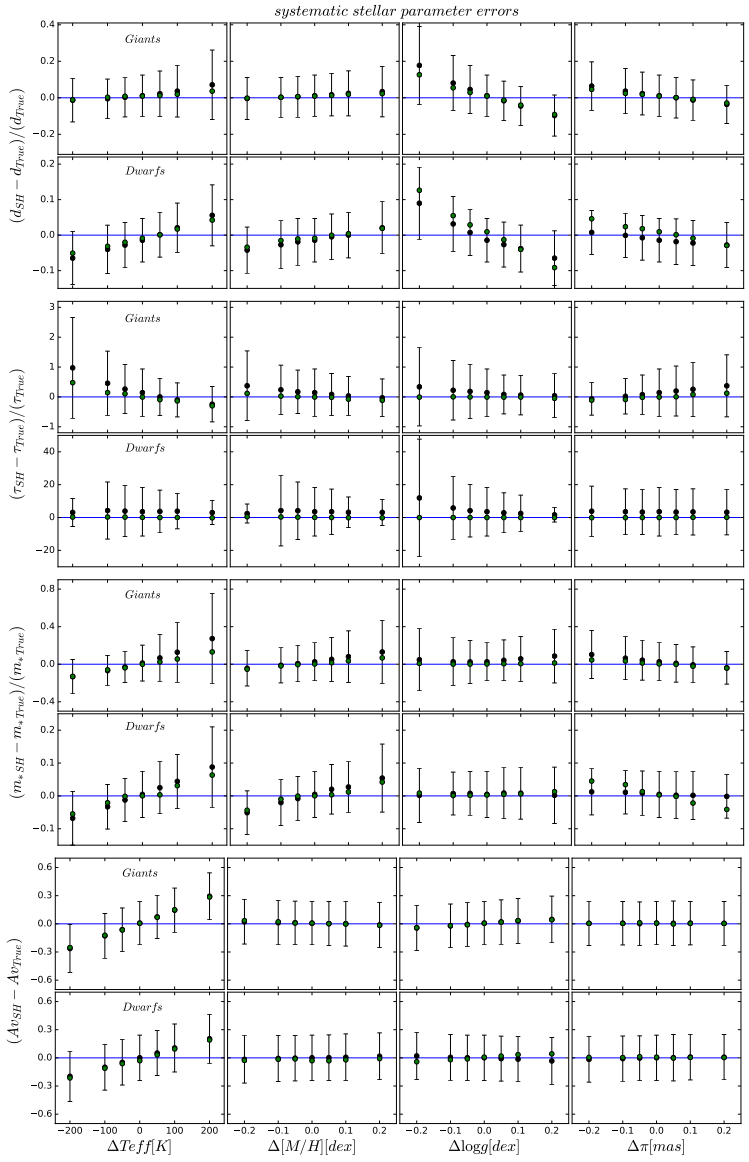

Figure 6. Relative errors per parameter (First two rows: d, third and fourth rows: τ, fith and sixth rows: m_{ast}, seventh and eighth rows: A_V) obtained when different systematic offsets are introduced to the stellar parameter at a time. For this test we use the simulated PARSEC sample with high-resolution errors, but only 500 stars. The panels show the results for giant stars with $\log g < 4$, and dwarf stars with $\log g > 4$ separately. From the left, the first column shows the results for offsets to $T_{\rm eff}$, the second column shows the offsets to [M/H], the third column shows the offsets to $\log g$, and the last column shows the offsets to parallax π. In each panel, the black (green) dots represent the mean (median) of the distribution of relative errors in each parameter, whereas the standard deviation from the mean is shown as the error bars.

able masses, Gaia parallaxes, metallicities, and magnitudes in at least one the following filter systems: Tycho (Høg et al. 2000), APASS (Henden & Munari 2014), Strömgren (Casagrande et al. 2014) and 2MASS (Cutri et al. 2003). Their distances and extinctions were estimated by performing fits to the broad-band photometric spectral energy distributions of the binary systems. The range of the parameters is described in Table 3. Although most of the parameters are individual for each star, the magnitudes are systemic; these magnitudes describe the binary system, not each star individually. This can include a bias in our likelihood, and as most of the sample is made by systems with similar massas, this will affect both primary and secondary stars, though the effect would be grater on the secondary stars. It is very important to proceed with this test, since approximately 50% of Solar-type field stars are binary or multiple systems (Raghavan et al. 2010; Moe & Di Stefano 2017), and most of them are photometricaly unresolved.

To run StarHorse we only select stars with available masses and limit the distance to 1 kpc. Figure 8 compares the StarHorse results for these stars with the ones of Stassun & Torres (2016). The StarHorse distances are in general underestimated in relation to the ones estimated by Stassun & Torres (2016). Most of our distance estimates are smaller by 20% (see Table 4), the effect being larger for the secondary members. This is probably a direct result of the systemic magnitudes we are using, since each star is assigned a brighter magnitude than it actually is, the amplitude of the effect being larger for secondaries. Therefore, our code will tend to match it with models at nearer distances. The masses estimated by StarHorse are in reasonable agreement with the reference sample, as shown in Table 4: 50% of the stars present relative errors smaller then 10%. We should keep in mind that the surface gravities for this EBs sample are based on the quoted radii and masses. The estimated extinction values do not present systematic deviation with the extinction given by Stassun & Torres (2016), but as the extinction strongly depends on the distance models, they also should be affected by the systemic magnitudes.

5.2 Asteroseismology: CoRoGEE

We also use the CoRoT-APOGEE sample (CoRoGEE; Anders et al. 2017) to evaluate the accuracy of our StarHorse results. CoRoGEE contains seismic measurements (from CoRoT) combined with high resolution spectra (from APOGEE) for more then 600 stars, this sample has also estimates of distance, age, mass, and A_V from the PARAM code. They cover a wide range of Galactocentric distances, metallicities, and ages (see Table 3), but are all red giants stars. To run StarHorse, we use as input the atmospheric parameters and total metallicity given by APOGEE, and the parallaxes as the inverse of the distance given by PARAM. We then compare our estimates with the ones from PARAM. The comparison is shown in Figure 9. The estimated distances are in excellent agreement (upper left panel), since the well-constrained input parallaxes are used by StarHorse when building the marginalized distance PDF for each star.

The upper right panel of Figure 9 shows the comparison between StarHorse and PARAM ages. The discreteness of our age grid is visible in the plot. The scatter is large, but most of the stars have ages that agree within ±50% of each other. The median and 84%-ile positions in the distribution of age discrepancies are 12% and 65%, respectively (Table 4). As in the case of the EBs, StarHorse tends to yield larger ages than those based on asteroseimology, but this time with a smaller median systematic (16%). In general, the results are quite similar to those from the previous section. This is also true for the extinction estimates, shown in the bottom right panel of Fig. 9. The mass estimates tend to show a better agreement in the case of CoRoGEE, with no systematic trend and smaller errors (median value of 4%) when compared to the EBs.

5.3 The OCCASO Clusters

As a third comparison sample, we use the data from the Open Clusters Chemical Abundances from Spanish Observatories (OCCASO) sample (Casamiquela et al. 2016, 2017). This sample contains a total of 128 stars from 18 clusters, covering Galatocentric distances out to 6 kpc, and a small range in metallicity. OCCASO contains only red clump stars, for a better spectroscopic resolution in spectroscopy. The age and distance estimates for these clusters are based on isochrone fitting, with a typical uncertainty of 0.2 mag in distance modulus and a mean age uncertainty of 0.2 Gyr. The input parameters used for StarHorse were parallaxes, converted from the isochrone distances, metallicities, and atmospherical parameters for each star from high-resolution spectroscopy from OCCASO survey; the mean uncertainty on these parameters can be seen in Table 3.

Figure 10 shows the comparison to StarHorse distances and ages. Each point is a star, for which the cluster's distance and age are attributed. The distances agree with no systematics and median (84%-ile) discrepancies of 2% (13%). Only a few of stars from the most distant cluster resulted with StarHorse distances significantly above the one from isochrone fitting. The ages exhibit larger relative discrepancies (31% and 63%, respectively for the 50%-ile and 84%-ile positions). We notice from the figure that the stars with a high discrepancy on distance also results in a high discrepancy in age (dark blue points), these points belong to the NGC 6791 cluster – one of oldest open clusters in the Milky Way. Still, for most of the stars the age estimates are consistent within the relatively large error bars.

6 RELEASED DATA PRODUCTS

We applied StarHorse to a few spectroscopic surveys together with astrometric and photometric measurements to deliver public distances and extinction catalogues. For the moment we are not releasing ages and masses because their estimates are still subject to considerable improvement. Among the several spectroscopic surveys available to the community, we chose among those that have been more widely used and which have high to medium resolution. All catalogues are available to the community via the LineA web page[4]. As our method is subject to further improve-

[4] http://www.linea.gov.br/020-data-center/acesso-a-dados-3/spectrophotometric-distances-starhorse-code/

Table 4. Results of the external validation tests. We report the percentiles of the modulus of the relative deviation distribution and the median of the relative deviation distribution for each parameter estimated by `StarHorse`. Data are shown for all reference samples used.

Sample	Parameter	P_5	P_{16}	P_{50}	P_{84}	P_{95}	median
PARSEC	d	0.005	0.015	0.063	0.163	0.258	0.0
high-res	τ	0.002	0.109	0.350	0.972	4.203	0.0
	m_*	0.001	0.012	0.074	0.222	0.391	0.0
	Av	0.005	0.014	0.048	0.107	0.162	0.0
PARSEC	d	0.005	0.016	0.060	0.172	0.289	-0.001
low-res	τ	0.014	0.110	0.398	1.120	4.550	0.002
	m_*	0.003	0.017	0.083	0.247	0.429	-0.001
	Av	0.016	0.049	0.169	0.354	0.499	0.004
TRILEGAL	d	0.007	0.023	0.079	0.171	0.240	-0.04
all priors	τ	0.017	0.054	0.188	0.516	0.937	0.11
	m_*	0.006	0.019	0.063	0.132	0.206	-0.04
	Av	0.003	0.012	0.043	0.099	0.162	0.007
Detached	d	0.001	0.002	0.017	0.041	0.047	-0.015
Eclipsing Binaries	τ	0.009	0.022	0.246	0.764	1.94	0.22
	m_*	0.008	0.033	0.124	0.165	0.194	-0.12
	Av	0.017	0.030	0.072	0.186	0.354	-0.07
Other	d	0.032	0.071	0.178	0.298	0.419	-0.178
Eclipsing Binaries	m_*	0.005	0.021	0.099	0.168	0.23	0.048
	Av	0.021	0.044	0.130	0.269	0.338	0.075
CoRoGEE	d	0.000	0.001	0.003	0.008	0.014	0.0
	τ	0.013	0.047	0.120	0.650	1.253	0.16
	m_*	0.003	0.011	0.043	0.097	0.164	0.0
	Av	0.009	0.024	0.070	0.158	0.270	-0.04
OCCASO	d	0.000	0.001	0.0244	0.130	0.310	0.0
cluster members	τ	0.028	0.090	0.310	0.626	0.968	-0.07

ments (e.g. incorporating new Gaia information, new stellar tracks with denser model grids, future releases of the adopted databases, and new extinction priors), this will lead to new versions of the released data, therefore, we suggest the reader to check for next releases at the LineA web page.

The following subsections explain the procedure used to determine distances and extinctions for each spectroscopic survey. We applied `StarHorse` in these samples with all priors described in §3, and in all cases the following corrections were made to each survey catalogue:

(i) *Polish photometry*
In some few cases in which a 2MASS (Cutri et al. 2003) magnitude of a star exists, but the associated uncertainty is -9999.99, we substitute this value by 0.2 mag. Similarly, if the quoted APASS magnitude uncertainty is 0, we set it to be 0.15 mag, and introduce an error floor of 0.02 mag.

(ii) *Correct metallicities for [α/Fe]-enhancement*
Since the PARSEC 1.2S stellar models do not yet include models with non-Solar [α/Fe] ratio, we correct for this effect in the data, following Salaris et al. (1993), by defining a total metallicity [M/H] as:

$$[\mathrm{M/H}] = [\mathrm{Fe/H}] + \log(0.638 \cdot [\alpha/\mathrm{Fe}]^{10} + 0.362)$$

$$\sigma_{[\mathrm{M/H}]} = \sqrt{\sigma^2_{[\mathrm{Fe/H}]} + \sigma^2_{[\alpha/\mathrm{Fe}]}}$$

6.1 APOGEE Catalogues

The APOGEE-2 survey (Majewski et al. 2017) is a program from the Sloan Digital Sky Survey (SDSS-IV, Blanton et al. 2017). It is a spectroscopic survey conducted in the near infrared, with high resolution ($R \sim 20,500$), and high signal-to-noise ($S/N > 100$). It maps the Galaxy through all populations and it has targeted, as of its latest release (DR14; Abolfathi et al. 2017), about 270,000 stellar spectra. As a near infrared survey of high resolution, APOGEE has the advantage to study with more detail the stars located in the dusty regions of our Galaxy, such as the Bulge and Disk. We applied StarHorse to the latest APOGEE release, DR14.

6.1.1 APOGEE DR14 ASPCAP

We used the APOGEE DR14 allStar summary catalogue (`allStar-l31c.2.fits`[5]). The file contains photometry in the 2MASS JHK_s passbands (Cutri et al. 2003), as well as chemical abundances and atmospheric parameters derived by the APOGEE Stellar Parameters and Chemical Abundances (ASPCAP; García Pérez et al. 2016). Starting from this file we took the following pre-processing steps before running `StarHorse`:

[5] available at `https://data.sdss.org/sas/dr14/apogee/spectro/redux/r8/allStar-l31c.2.fits`

Table 5. General description of the release distances and extinctions

Column	Description	units
OBJECT ID	Survey's object ID name	
glon	Galactic longitude	degrees
glat	Glactic latitude	degrees
dist05	5th percentile of the stars's distance PDF	kpc
dist16	16th percentile of the stars's distance PDF	kpc
dist50	50th percentile of the stars's distance PDF	kpc
dist84	84th percentile of the stars's distance PDF	kpc
dist95	95th percentile of the stars's distance PDF	kpc
meandist	Mean of the stars's distance PDF	kpc
diststd	standard deviation of the stars's distance PDF	kpc
AV05	5th percentile of the stars's extinction PDF	mag
AV16	16th percentile of the stars's extinction PDF	mag
AV50	50th percentile of the stars's extinction PDF	mag
AV84	84th percentile of the stars's extinction PDF	mag
AV95	95th percentile of the stars's extinction PDF	mag
meanAV	Mean of the star's extinction PDF	mag
stdAV	Standard deviation of the stars's extinction PDF	mag
SH_INPUTFLAGS	`StarHorse` flags regarding the input data	
SH_OUTPUTFLAGS	`StarHorse` flags regarding the output data	

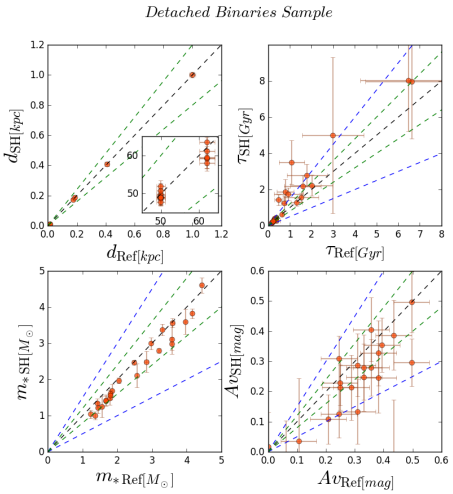

Figure 7. Comparison between our distance (upper left panel), age (upper right panel), mass (lower left), and extinction (lower right) results with those from asteroseismology and the PARAM code for the sample of Ghezzi & Johnson (2015) binaries. The black dashed line is the identity line. The green dashed lines correspond to ±20% deviates, whereas the blue dashed lines (in the last three panels only) correspond to ±50%. The insert on the bottom right shows the same comparison for the LMC/SMC stars.

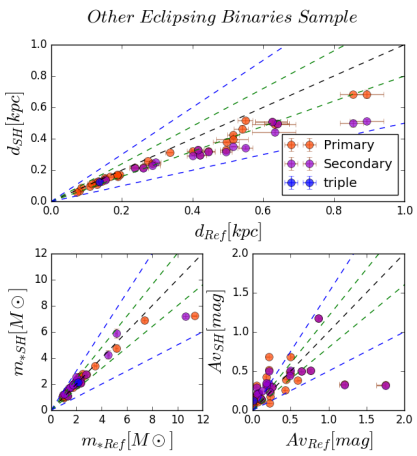

Figure 8. Comparison between our distance (upper panel), mass (left lower panel) and extinction (right lower panel), results with those from the EB sample of Stassun & Torres (2016). The dashed lines correspond to the same deviates as in Figure 7. The legend shows the orange dots representing the primary star, the purple dots the secondary star, and the blue dots represents detected triple systems.

(i) *Cross-match with photometry and astrometry*
Using TOPCAT (Taylor 2005), we did a positional crossmatch so as to add information from APASS DR9 (Henden & Munari 2014) (207,604 matches) and *Gaia* DR1/TGAS (Gaia Collaboration et al. 2016) (46,033 matches). Our crossmatch used a maximum separation of 5 arcsec.

(ii) *Selecting reliable results*
We discarded sources with ASPCAP flags containing the words "BAD" or "NO_ASPCAP". In addition, we selected only sources with valid 2MASS H magnitudes. This resulted in a total of 226,323 stars.

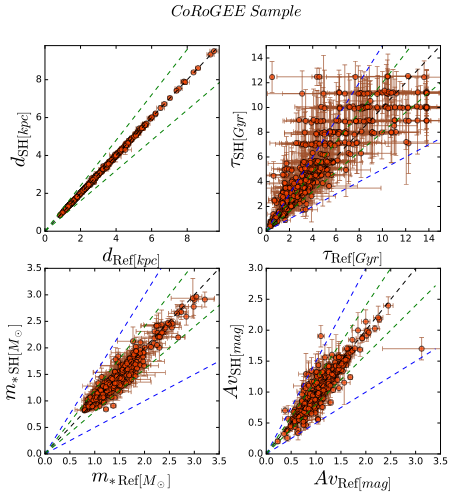

Figure 9. Same panels as in Figure 7, but now showing the comparison to the CoRoGEE sample.

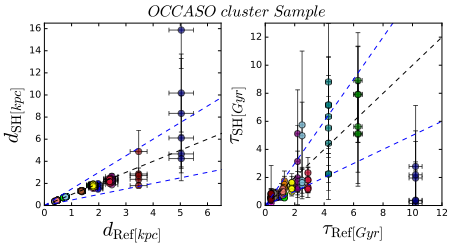

Figure 10. Same as the upper panels in Figures 7 and 9, but now showing the comparison of determined distances and ages to those for the star cluster sample from OCCASO, described in Sec. 5.3. The stars in the figure are coloured as an identification of their cluster host. In this figure we show only the identity and ±50% deviating lines.

(iii) *Using uncalibrated ASPCAP results*
When no calibrated ASPCAP results for one or more spectroscopic parameters are available (stars outside the calibration ranges; e.g., $\log g$ values for dwarfs), we use uncalibrated ASPCAP results. For those objects we inflated the uncertainties. Our ad-hoc conservative uncertainty estimates for these cases amount to 150 K in $T_{\rm eff}$, 0.3 dex in $\log g$, 0.15 dex in [M/H], and 0.1 dex in [α/M].

(iv) *A_V prior*
As priors for the V-band extinction we used the APOGEE targeting extinction values (Zasowski et al. 2013), derived by the RJCE method (Majewski et al. 2011), by setting $A_{V,\rm prior} = A(K_s)_{\rm Targ}/0.12$. When RJCE estimates were not available, we used $E(B-V)$ estimates from (Schlegel et al. 1998) to estimate the prior A_V. As explained in Sec. 3.2.2, the posterior A_V values are allowed to lie in a very broad interval around the prior values.

We then applied `StarHorse` to the resulting catalogue. Our results are available through an SDSS-IV value-added catalogue (VAC) of APOGEE stellar distances, as part of SDSS DR14[6] and on the Line web-page. The output format of this catalogue is described in Table 5. Figure 11 summarises the results for APOGEE DR14. Figure 12 shows the associated uncertainty distributions.

6.1.2 *APOGEE DR14 Cannon*

As the APOGEE DR14 also contains stellar parameters and chemical abundances derived by the data driven method called Cannon (Ness et al. 2015; Casey et al. 2016), we also applied StarHorse with this input. We used the APOGEE DR14[7] allStar summary catalogue (`allStarCannon-l31c.2.fits`). Which contains the atmospheric stellar parameters, chemical abundances and its uncertainties. Starting from this file we did the following steps to prepare a input to `StarHorse`:

(i) *Cross-match with photometry and astrometry*
We carried out a positional cross match, using TOPCAT (Taylor 2005), with photometry from APASS (Henden & Munari 2014) and from 2MASS (Cutri et al. 2003).

(ii) *Av Prior*
As priors for the V-band extinction we used the APOGEE targeting extinction values (Zasowski et al. 2013), derived by the RJCE method (Majewski et al. 2011), by setting $A_{V,\rm prior} = A(K_s)_{\rm Targ}/0.12$.

6.2 The Gaia-ESO sample

The *Gaia*-ESO survey (GES Gilmore et al. 2012) is a large public spectroscopic survey with high resolution that covers all Milky Way components and open star clusters of all ages and masses. The final GES release is expected to include about 10^5 stars.

We downloaded the *Gaia*-ESO data release 3 (DR3) from the ESO catalogue facility[8]. This catalogue contains a total of 25533 stars, including the Milky-Way field, open clusters, and calibration stars. The catalogue contains 100 columns, from which we selected the necessary information to run `StarHorse`: atmospheric parameters, elemental abundances, and 2MASS JHK_s pass-bands (Cutri et al. 2003). From this catalogue we proceeded with the following steps, before applying `StarHorse`.

(i) *Select only field stars and reliable sources:*
From this catalogue we selected only Milky Way field stars,

[6] `http://www.sdss.org/dr14/irspec/spectro_data/`
[7] `http://www.sdss.org/dr14/irspec/spectro_data/`
[8] `http://www.eso.org/rm/api/v1/public/releaseDescriptions/91`

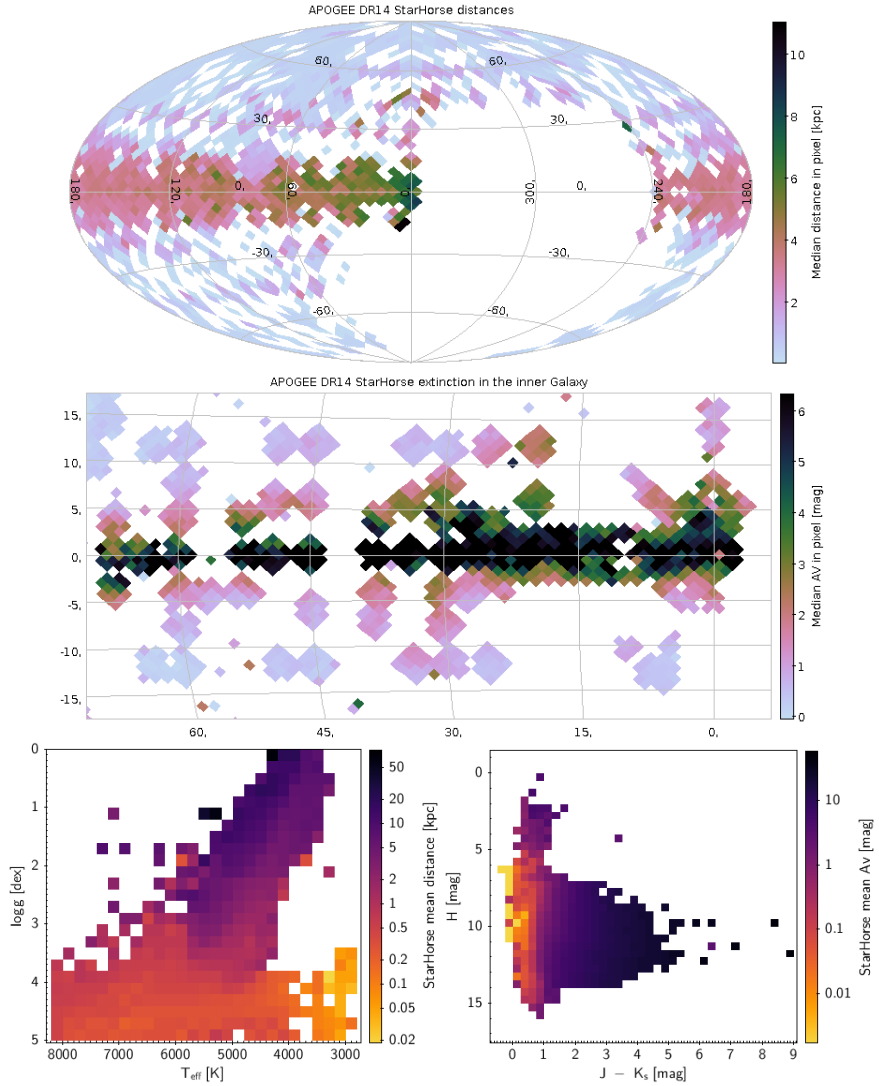

Figure 11. Illustration of the APOGEE DR14 distance and extinction results from StarHorse. Top panel: Aitoff projection of median APOGEE distances per HealPix cell in Galactic coordinates. Middle panel: Resulting median A_V per HealPix cell in the inner Galaxy. Bottom left panel: Spectroscopic Hertzsprung-Russell diagram, colour-coded by median distance in each pixel. Bottom right panel: 2MASS colour-magnitude diagram, colour-coded by median extinction in each pixel.

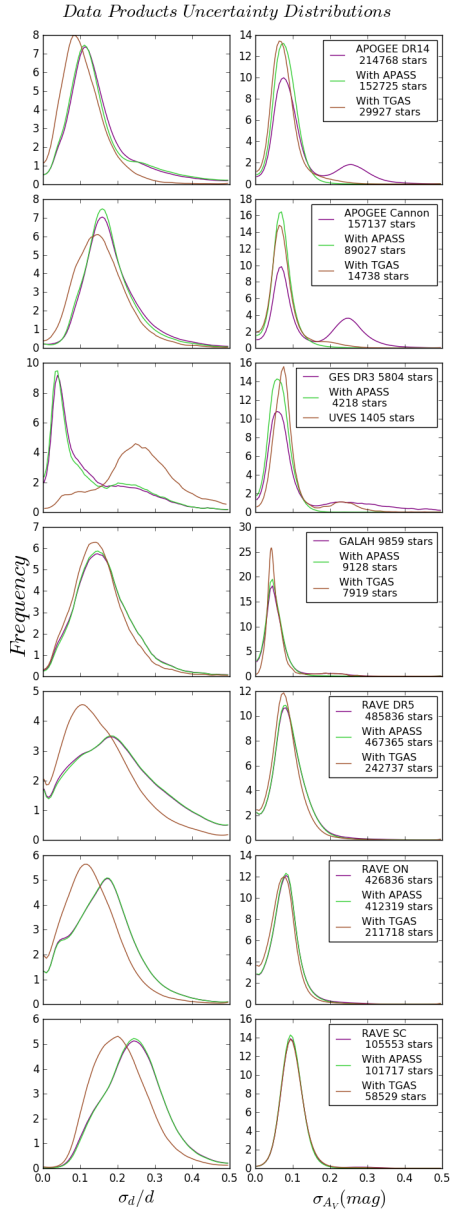

Figure 12. `StarHorse` relative distance (left panels) and absolute extinction (right panels) uncertainty distributions for all release data products. The legend specifies the stars with available APASS photometry, parallaxes from TGAS or UVES spectroscopy (GES sample).

which are the main targets intended for `StarHorse`. This leaves us with 7870 stars. We then adopted the following quality criteria: relative errors in Teff less than 5%; errors in logg lower than 0.4 dex; and errors in metallicity lower than 0.2 dex, with no cuts in the abundances. From the 7870 field stars, 6316 of them meet these criteria.

(ii) *Calculate an overall* $[\alpha/Fe]$ *abundance:*
The PARSEC models do not list individual elemental abundances, only the total metallicity value, [M/H]. The models do not include non-Solar abundances in α elements either. Therefore, we converted the GES abundances in the total metallicity [M/H] before running `StarHorse`. For that purpose, we calculated the overall [α/Fe] abundance as follows:

$$[\alpha/\mathrm{Fe}] = \frac{1}{n}\sum_{i=1}^{n}[\mathrm{X_i/H}] - [\mathrm{Fe/H}],$$

where X_i refers to the elements O, S, Ti, Ca and Mg, and the [X_i/H] abundances were calculated using the solar values from Asplund et al. (2009). The error in [α/Fe] was propagated in quadrature from the error on each elemental abundance and the error in [Fe/H].

(iii) *Cross-match with photometry*:
To obtain more precise and reliable extinction estimates we decided to include APASS (Henden & Munari 2014) magnitudes for this sample. For this we carried out a positional crossmatch with APASS DR9 (Henden & Munari 2014) using TOPCAT (Taylor 2005), with a maximum sparation of 1 arcsec. Of the 6316 stars, 5719 stars have APASS magnitudes.

(iv) A_V Prior:
No $A_V$prior was applied to this sample, therefore the posterior probability function for A_V always ranges from 0 to 3 (mag).

After carrying out these steps, we used this final catalog with 6316 stars as input to `StarHorse`. The code delivered an output catalog with 6011 stars with available distances and extinctions. The columns of the released distances and extinction catalogue are shown in Table 5, and the uncertainties distribution are shown in Figure 12.

6.3 GALAH sample

The Galactic Archaeology with HERMES (GALAH; Martell et al. 2017) is a spectroscopic survey that will target about 1 million stars with the high-resolution ($R \sim 28,000$) instrument High Efficiency and Resolution Multi-Element Spectrograph (HERMES; de Silva et al. 2012), at the Anglo-Australian Telescope (AAT). The main goal of the project is to provide a detailed star-formation history for the thick and thin disks. Therefore, the survey covers mainly the disk, but it also has some fields towards the bulge and halo. A first public data release of GALAH is already available. We then applied `StarHorse` to estimate distances and extinction for GALAH DR1 stars. The catalogue[9] contains 10680 stars

[9] https://cloudstor.aarnet.edu.au/plus/index.php/s/OMc9QWGG1koAK2D

with [Fe/H], [α/Fe], log g, and $T_{\rm eff}$ measurements derived by the Cannon method (Ness et al. 2015). We proceeded with the following steps to have an input catalogue ready for StarHorse:

(i) *Stellar parameter uncertainties*
The GALAH DR1 catalogue does not provide individual uncertainties for the stars. We therefore used the values recommended by Martell et al. (2017): σ([Fe/H]) = 0.056 dex, $\sigma(\log g)$ = 0.17 dex and $\sigma(T_{\rm eff})$ = 51 K. As there is no mention of the uncertainty in [α/Fe], so we assumed the error to be same as for σ[Fe/H].

(ii) *Cross-match with photometry and astrometry*:
Since the GALAH DR1 catalog has stars in commom with the *Gaia* DR1, we carried out a positional crossmatch with *Gaia* using TOPCAT (Taylor 2005), with a maximum sparation of 1 arcsec. From the 10680 DR1 stars, 7919 stars have parallax available. We obtained photometry for the sample by crossmatching with the 2MASS (Cutri et al. 2003) (10680 matches) and APASS (Henden & Munari 2014) (9263 matches) catalogues.

(iii) *Av Prior*
We use the reddening given by the GALAH DR1 catalogue, which is derived by comparison of absolute magnitudes with the apparent magnitude V from APASS (Henden & Munari 2014) and J magnitude from 2MASS(Cutri et al. 2013). We assumed then that $A_V = 3.1E(B-V)$.

After these steps were completed, we used this final file as input to StarHorse and derived distances and extinctions. The code returned 10,623 distances and extinctions. The columns for the released catalogue are described in Table 5 and the uncertainty distribution is shown in Figure 12.

6.4 The RAVE catalogues

The RAdial Velocity Experiment (RAVE, Steinmetz et al. 2006) is one of the largest spectroscopic surveys of the Milky Way. RAVE has already delivered spectra for almost 500K stars, that were randonly targeted in an area of 20K square degrees of the Galactic Southern Hemisphere. In addition, RAVE is currently the survey that contains the largest number of stars in common with TGAS (∼ 200K stars). The survey works with a multi-object spectrograph deployed on 1.2-m UK Schmidt Telescope of the Australian Astronomical Observatory (AAO). The spectra have a medium resolution of ($R \sim 7,500$) and cover the Ca-triplet region (8410-8795 Å). Given that RAVE has a medium resolution, is pioneering among the large spectroscopic surveys, covers a large area, and has the largest overlap with the Gaia sample, we decided to apply StarHorse to the entire survey, and to make the estimated distances and extinctions available to the community. The following subsections explain how we proceed with the RAVE input catalogues to execute StarHorse and the description of the released distances-extinction catalogues. All RAVE catalogues were downloaded from the RAVE website[10].

[10] https://www.rave-survey.org/project/

6.4.1 *The RAVE DR5 catalogue*

The data release 5 (DR5 Kunder et al. 2017) is the lastest RAVE data release. It contains spectra for 483,330 stars. We downloaded the publicly released catalogue called RAVE_DR5, which contains spectral parameters and radial velocities derived by the SPARV pipeline (Zwitter et al. 2008; Siebert et al. 2011). The catalogue also contains astrometry from *Gaia*-DR1 (215,590), and photometry from 2MASS and APASS. We note that very recently, McMillan et al. (2017) updated the DR5 catalogue parameters and derived distances using feedback from the Gaia DR1 parallaxes, but our VAC presented here is based on the public DR5 data. From this catalogue, we proceeded with the following steps before running StarHorse:

(i) *Spectral parameters*
We use the calibrated atmospheric parameters, which are named in the catalogue as $\rm Teff_{NK}$, $\rm logg_{NK}$, $\rm Met_{NK}$. For the uncertainties, if the error spectral analysis is available, we use the maximum between the two values: $\sigma\rm Teff_K$ and $\rm StdDevTeff_K$, otherwise we use the maximum between: 70K and σ $\rm Teff_K$. We worked analogously with the other parameters.
(ii) A_V *prior*
As explained in section 3.2.2, we can use a prior value of extinction to build the A_V posterior probability function. We use as extinction prior in V-band the maps of $E(B-v)$ from Schlegel et al. (1998) for this catalogue.

6.4.2 *RAVE-SC catalogue*

The RAVE-SC catalogue has stars from DR5 with gravity from seismic calibrations (Valentini et al. 2017), therefore this sample is only compose by giants. We downloaded the catalogue named as RAVE_Gravity_SC. Step 1 from the previous subsection 6.4.1 was also applied to this sample. We use the overall [α/Fe] abundance and the [Fe/H], given by the catalogue to calculate a total metallicity as defined by (Salaris et al. 1993), with a fixed uncertainty of 0.2 dex. The atmospheric parameters were used as they were given by the catalogue; we use the following temperature and surface gravity columns: Teff_IR and logg_SC. For the A_V prior we use the Schlegel et al. (1998) $E(B-V)$ maps.

6.4.3 *RAVE-on catalogue*

The RAVE-on catalogue (Casey et al. 2017) has stars from DR5 with parameters derived by the Cannon method (Casey et al. 2016). We downloaded the catalogue named as RAVE-ON. The atmospheric parameters and [Fe/H] were used directly from this catalogue. The following steps were applied before applying StarHorse:

(i) *Calculate an overall* $[\alpha/Fe]$ *abundance*
The Cannon provides the individual abundances for the stars. We then calculated [α/Fe] as the simple average between the individual abundances when they are available, exactly as described in section 6.2, with X_i as O, Mg, Ca, and Si.
(ii) A_V Prior:
No $A_V$prior was applied to this sample, therefore the posterior probability function for A_V always ranges from 0

to 3 (mag).

6.5 StarHorse FLAGS

All released data products catalogues have two columns that describe the StarHorse input data, SH_INPUTFLAGS, and the StarHorse output data, SH_OUTPUTFLAGS, as shown in Table 5. The input flags specify which parameters were used in the likelihood calculation to estimate the distances and extinctions given. For example, if the temperature was available for that star a TEFF flag will appear, and if TEFF was not available in the calculation a uncalTEFF flag will appear. The other parameters are specified as follows in the input flag: LOGG (surface gravity), PARALLAX (parallax), MH (metallicity), JHKs (2Mass filters) and BVgri (APASS filters). If the input flag contains ALPHAM it means that the alpha elements were available in the calculation of the total metallicity of the star. The input flags also indicate you if we use a A_V prior as the AVprior flag. The output flags tell us if the number of models which have converged in the likelihood calculation is too small. If less then 10 models are consistent with the star a NUMMODELS_BAD flag will appear, while if the number of models is between 10 and 30 a NUMMODELS_WARM flag will appear. The output flags also indicate if the estimated extinction is negative (NEGATIVE_EXTINCTION_WARN), if it is too high (HIGH_EXTINCTION_WARN), or if the estimated extinction has a bright 2Mass source (EXTINCTION_BAD_BRIGHT2MASS).

7 SUMMARY AND FUTURE PERSPECTIVES

We have presented a code that computes distances, ages, masses, and extinctions for field stars with photometric, spectroscopic, and astrometric data. It is based on Bayesian inference, computing the marginal posterior distributions for the data given a set of stellar models. The code represents a significant improvement over the one presented by Santiago et al. (2016) in several aspects. The most important one is the ability to estimate ages, masses, and extinction, in addition to the spectrophotometric distances presented by those authors. The updated code, which we call StarHorse, is also capable of incorporating the parallax as an additional observational quantity in the statistical analysis (Figure 1). Updated spatial, metallicity, and age priors for the Galactic components, now including the bulge as well, are presented (Table 1). In addition, StarHorse is now more flexible in terms of the input data and the choice of observational quantities to be used within them.

The new code was validated using simulated and real stars. These latter are samples with reliable parallax (or distance) data, including field giants with asteroseismic data, EBs used as benchmarks for stellar evolutionary codes, or cluster stars with well-known distances and ages, usually from isochrone fitting, often in combination with spectroscopic data. For EBs that are not detached, the distances present an offset in relation to the reference ones, our distances being usually smaller by 20% in this specific case. The discrepancy is larger for secondary stars than for the primary ones, which is what one expects from using systemic photometric measurements. In all cases, age is the single most difficult parameter to infer, yielding median errors that range from 12% to 35% for quality spectrophotometric data, depending on the sample (Table 4). Errors larger than 100% in age may result for $\simeq$ 15% of the stellar models, most of them younger than $\tau \simeq 1$ Gyr. In a realistic flux-limited sample, as simulated by the TRILEGAL code or for real stars, the fraction of such catastrophic age errors is reduced to $\simeq$ 5% of the stars. Our results for stellar ages, either based on simulated or real stars, also indicate a systematic trend of StarHorse overestimating ages by $10-20\%$.

As for spectrophotometric masses, we obtain consistent results over all validation samples used, in the sense that errors $< 20\%$ are observed for most (84%) of the stars in any sample. The median error varies depending on the quality of the parallax used as a constraint. For typical *Gaia*-TGAS errors of 0.3 mas, the typical distance errors are around 15%. For real stars used as reference, median StarHorse A_V errors are of 0.07 mag, with the $84\% - ile$ error at $0.15-0.20$ mag. For TRILEGAL and PARSEC synthetic stars, the relatice errors are a bit smaller, around 0.04 mag.

We note that the error estimates based on comparison to real samples may be overestimated, considering that the some of the discrepancy may be attributed to the methods used to obtain the reference quantities for comparison. In fact, Rodrigues et al. (2017) report that ages and masses from asteroseismology are typically obtained with a precision of 19% and 5%, respectively, which are comparable to the errors we quote in this analysis.

StarHorse has already been used to infer distances and extinction values for stars from APOGEE DR14. These parameters, in turn, may be used in connection to APOGEE abundances and radial velocities, to study the properties of the main Galactic populations, and their spatial variations, as was previously done by Anders et al. (2014), and Fernández-Alvar et al. (2016) using distances from Santiago et al. (2016). For more local samples, such as *Gaia*-TGAS and RAVE, reliable parallax information can be included in the Bayesian method to yield masses and ages, as validated in this paper, allowing for a more detailed modelling of the chemo-dynamical history of our Galaxy (Anders et al. 2017).

Finally, we have run StarHorse on different public catalogs from the RAVE collaboration, as well as on GES, and GALAH public data releases. These are available for download at the LIneA web site.[11]

ACKNOWLEDGEMENTS

The StarHorse code is written in python 2.7 and makes use of several community-developed python packages, among them astropy (Astropy Collaboration et al. 2013), ezpadova[12], numpy and scipy (Oliphant 2007), and matplotlib (Hunter 2007). The code also makes use of the photometric filter database of VOSA (Bayo et al. 2008), developed under

[11] http://www.linea.gov.br/020-data-center/acesso-a-dados-3/spectrophotometric-distances-starhorse-code/
[12] https://github.com/mfouesneau/ezpadova

the Spanish Virtual Observatory project supported from the Spanish MICINN through grant AyA2011-24052.

We thank Eddie Schlafly (LBL) as well as the anonymous referee for various useful comments that helped improving the manuscript.

We thank Laia Casamiquela for providing data from the OCCASO survey.

Funding for the SDSS Brazilian Participation Group has been provided by the Ministério de Ciência e Tecnologia (MCT), Fundação Carlos Chagas Filho de Amparo à Pesquisa do Estado do Rio de Janeiro (FAPERJ), Conselho Nacional de Desenvolvimento Científico e Tecnológico (CNPq), and Financiadora de Estudos e Projetos (FINEP).

Funding for the Sloan Digital Sky Survey IV has been provided by the Alfred P. Sloan Foundation, the U.S. Department of Energy Office of Science, and the Participating Institutions. SDSS-IV acknowledges support and resources from the Center for High-Performance Computing at the University of Utah. The SDSS web site is www.sdss.org.

SDSS-IV is managed by the Astrophysical Research Consortium for the Participating Institutions of the SDSS Collaboration including the Brazilian Participation Group, the Carnegie Institution for Science, Carnegie Mellon University, the Chilean Participation Group, the French Participation Group, Harvard-Smithsonian Center for Astrophysics, Instituto de Astrofísica de Canarias, The Johns Hopkins University, Kavli Institute for the Physics and Mathematics of the Universe (IPMU) / University of Tokyo, Lawrence Berkeley National Laboratory, Leibniz-Institut für Astrophysik Potsdam (AIP), Max-Planck-Institut für Astronomie (MPIA Heidelberg), Max-Planck-Institut für Astrophysik (MPA Garching), Max-Planck-Institut für Extraterrestrische Physik (MPE), National Astronomical Observatory of China, New Mexico State University, New York University, University of Notre Dame, Observatário Nacional / MCTI, The Ohio State University, Pennsylvania State University, Shanghai Astronomical Observatory, United Kingdom Participation Group, Universidad Nacional Autónoma de México, University of Arizona, University of Colorado Boulder, University of Oxford, University of Portsmouth, University of Utah, University of Virginia, University of Washington, University of Wisconsin, Vanderbilt University, and Yale University.

This work has made use of data from the European Space Agency (ESA) mission *Gaia* (http://www.cosmos.esa.int/gaia), processed by the *Gaia* Data Processing and Analysis Consortium (DPAC, http://www.cosmos.esa.int/web/gaia/dpac/consortium). Funding for the DPAC has been provided by national institutions, in particular the institutions participating in the *Gaia* Multilateral Agreement. This work has also made use of data from *Gaia*-ESO based on data products from observations made with ESO Telescopes at the La Silla Paranal Observatory under programme ID 188.B-3002.

ABAQ and FA acknowledge support from the Leibniz Graduate School for Quantitative Spectroscopy at AIP, in particular the Outgoing and Incoming Mobility Programme. CC acknowledges support from DFG Grant CH1188/2-1 and from the ChETEC COST Action (CA16117), supported by COST (European Cooperation in Science and Technology). TCB acknowledges partial support from grant PHY 14-30152: Physics Frontier Center/JINA Center for the Evolution of the Elements (JINA-CEE), awarded by the US National Science Foundation.

REFERENCES

Abolfathi B., et al., 2017, ApJS, submitted, arXiv:1707.09322
Anders F., et al., 2014, A&A, 564, A115
Anders F., et al., 2017, A&A, 597, A30
Asplund M., Grevesse N., Sauval A. J., Scott P., 2009, ARA&A, 47, 481
Astropy Collaboration et al., 2013, A&A, 558, A33
Bayo A., Rodrigo C., Barrado Y Navascués D., Solano E., Gutiérrez R., Morales-Calderón M., Allard F., 2008, A&A, 492, 277
Bensby T., et al., 2013, A&A, 549, A147
Binney J., et al., 2014, MNRAS, 437, 351
Bland-Hawthorn J., Gerhard O., 2016, ARA&A, 54, 529
Blanton M. R., et al., 2017, AJ, 154, 28
Boeche C., et al., 2013, A&A, 559, A59
Boeche C., et al., 2014, A&A, 568, A71
Bovy J., Rix H.-W., Schlafly E. F., Nidever D. L., Holtzman J. A., Shetrone M., Beers T. C., 2016, ApJ, 823, 30
Bressan A., Marigo P., Girardi L., Salasnich B., Dal Cero C., Rubele S., Nanni A., 2012, MNRAS, 427, 127
Brogaard K., et al., 2016, Astronomische Nachrichten, 337, 793
Burnett B., Binney J., 2010, MNRAS, 407, 339
Burnett B., et al., 2011, A&A, 532, A113
Cardelli J. A., Clayton G. C., Mathis J. S., 1989, ApJ, 345, 245
Carlin J. L., et al., 2015, AJ, 150, 4
Casagrande L., et al., 2014, MNRAS, 439, 2060
Casamiquela L., et al., 2016, MNRAS, 458, 3150
Casamiquela L., et al., 2017, MNRAS, 470, 4363
Casey A. R., Hogg D. W., Ness M., Rix H.-W., Ho A. Q., Gilmore G., 2016, preprint, (arXiv:1603.03040)
Casey A. R., et al., 2017, ApJ, 840, 59
Chabrier G., 2003, PASP, 115, 763
Chiappini C., et al., 2015, A&A, 576, L12
Cutri R. M., et al., 2003, 2MASS All Sky Catalog of point sources.
Cutri R. M., et al., 2013, Technical report, Explanatory Supplement to the AllWISE Data Release Products
Dehnen W., Binney J., 1998, MNRAS, 294, 429
Deng L.-C., et al., 2012, Research in Astronomy and Astrophysics, 12, 735
Fernández-Alvar E., Allende Prieto C., Beers T. C., Lee Y. S., Masseron T., Schneider D. P., 2016, A&A, 593, A28
Fuhrmann K., 1998, A&A, 338, 161
Fuhrmann K., Chini R., 2017, ApJ, 834, 114
Gaia Collaboration et al., 2016, A&A, 595, A2
García Pérez A. E., et al., 2016, AJ, 151, 144
Ghezzi L., Johnson J. A., 2015, ApJ, 812, 96
Gilmore G., 2012, in Aoki W., Ishigaki M., Suda T., Tsujimoto T., Arimoto N., eds, Astronomical Society of the Pacific Conference Series Vol. 458, Galactic Archaeology: Near-Field Cosmology and the Formation of the Milky Way. p. 147
Gilmore G., et al., 2012, The Messenger, 147, 25
Girardi L., Groenewegen M. A. T., Hatziminaoglou E., da Costa L., 2005, A&A, 436, 895
Girardi L., et al., 2012, TRILEGAL, a TRIdimensional modeL of thE GALaxy: Status and Future. p. 165, doi:10.1007/978-3-642-18418-5_17
Gouda N., 2012, in Aoki W., Ishigaki M., Suda T., Tsujimoto T., Arimoto N., eds, Astronomical Society of the Pacific Conference Series Vol. 458, Galactic Archaeology: Near-Field Cosmology and the Formation of the Milky Way. p. 417

Hayden M. R., et al., 2015, ApJ, 808, 132
Haywood M., Di Matteo P., Lehnert M. D., Katz D., Gómez A., 2013, A&A, 560, A109
Henden A., Munari U., 2014, Contributions of the Astronomical Observatory Skalnate Pleso, 43, 518
Høg E., et al., 2000, A&A, 357, 367
Hunter J. D., 2007, Computing in Science and Engineering, 9, 90
Imai H., Burns R. A., Yamada Y., Goda N., Yano T., Orosz G., Niinuma K., Bekki K., 2016, preprint, (arXiv:1603.02042)
Kunder A., et al., 2017, AJ, 153, 75
Lagarde N., Robin A. C., Reylé C., Nasello G., 2017, A&A, 601, A27
Mackereth J. T., et al., 2017, MNRAS, 471, 3057
Maíz Apellániz J., 2006, AJ, 131, 1184
Majewski S. R., Zasowski G., Nidever D. L., 2011, ApJ, 739, 25
Majewski S. R., et al., 2017, AJ, 154, 94
Marigo P., Girardi L., Bressan A., Groenewegen M. A. T., Silva L., Granato G. L., 2008, A&A, 482, 883
Martell S. L., et al., 2017, MNRAS, 465, 3203
McMillan P. J., et al., 2017, preprint, (arXiv:1707.04554)
Melis C., Reid M. J., Mioduszewski A. J., Stauffer J. R., Bower G. C., 2014, Science, 345, 1029
Mikolaitis Š., et al., 2014, A&A, 572, A33
Mitschang A. W., De Silva G., Zucker D. B., Anguiano B., Bensby T., Feltzing S., 2014, MNRAS, 438, 2753
Moe M., Di Stefano R., 2017, ApJS, 230, 15
Ness M., Hogg D. W., Rix H.-W., Ho A. Y. Q., Zasowski G., 2015, ApJ, 808, 16
Nidever D. L., et al., 2014, ApJ, 796, 38
Oliphant T. E., 2007, Computing in Science and Engineering, 9
Raghavan D., et al., 2010, ApJS, 190, 1
Recio-Blanco A., et al., 2014, A&A, 567, A5
Robin A. C., Marshall D. J., Schultheis M., Reylé C., 2012, A&A, 538, A106
Robin A. C., Reylé C., Fliri J., Czekaj M., Robert C. P., Martins A. M. M., 2014, A&A, 569, A13
Rodrigues T. S., et al., 2014, MNRAS, 445, 2758
Rodrigues T. S., et al., 2017, MNRAS, 467, 1433
Ryan S. G., Norris J. E., Beers T. C., 1996, ApJ, 471, 254
Salaris M., Chieffi A., Straniero O., 1993, ApJ, 414, 580
Santiago B. X., et al., 2016, A&A, 585, A42
Schlafly E. F., et al., 2016, ApJ, 821, 78
Schlegel D. J., Finkbeiner D. P., Davis M., 1998, ApJ, 500, 525
Siebert A., et al., 2011, AJ, 141, 187
Stassun K. G., Torres G., 2016, AJ, 152, 180
Steinmetz M., et al., 2006, AJ, 132, 1645
Taylor M. B., 2005, in Shopbell P., Britton M., Ebert R., eds, Astronomical Society of the Pacific Conference Series Vol. 347, Astronomical Data Analysis Software and Systems XIV. p. 29
Valentini M., et al., 2017, A&A, 600, A66
Valle G., Dell'Omodarme M., Prada Moroni P. G., Degl'Innocenti S., 2015, A&A, 577, A72
Vanhollebeke E., Groenewegen M. A. T., Girardi L., 2009, A&A, 498, 95
Yanny B., et al., 2009, AJ, 137, 4377
Yong D., et al., 2016, MNRAS,
Zasowski G., et al., 2013, AJ, 146, 81
Zoccali M., et al., 2003, A&A, 399, 931
Zwitter T., et al., 2008, AJ, 136, 421
da Silva L., et al., 2006, A&A, 458, 609
de Jong R. S., Radburn-Smith D. J., Sick J. N., 2009, in Andersen J., Nordström B., Bland-Hawthorn J., eds, IAU Symposium Vol. 254, The Galaxy Disk in Cosmological Context. p. 19 (arXiv:0904.2777)
de Silva G. M., Heijmans J., Gers L., Zucker D., Aao Hermes Team 2012, in Aoki W., Ishigaki M., Suda T., Tsujimoto T., Arimoto N., eds, Astronomical Society of the Pacific Conference Series Vol. 458, Galactic Archaeology: Near-Field Cosmology and the Formation of the Milky Way. p. 415

APPENDIX A: ADDITIONAL SIMULATION RESULTS

Here we show the results of PARSEC simulations when parallaxes are not used to constrain distances or the likelihood. Figure A1 can then be compared to the case shown in the main body of the paper, Figure 3. All estimated parameters are subject to larger errors, especially A_V. The systematic distance and mass error dependances on true stellar age and mass become very pronounced when parallaxes are not used.

We also show the results of the TRILEGAL simulations for the case where no priors are adopted, to be compared to those shown in Figure 4, for the *All priors* case. Figure A2 show the results for TRILEGAL simulations with no spatial, MDF or ADF see §3.3.

APPENDIX B: ADDITIONAL DATA RELEASED ANALYSIS

This paper has been typeset from a TEX/LATEX file prepared by the author.

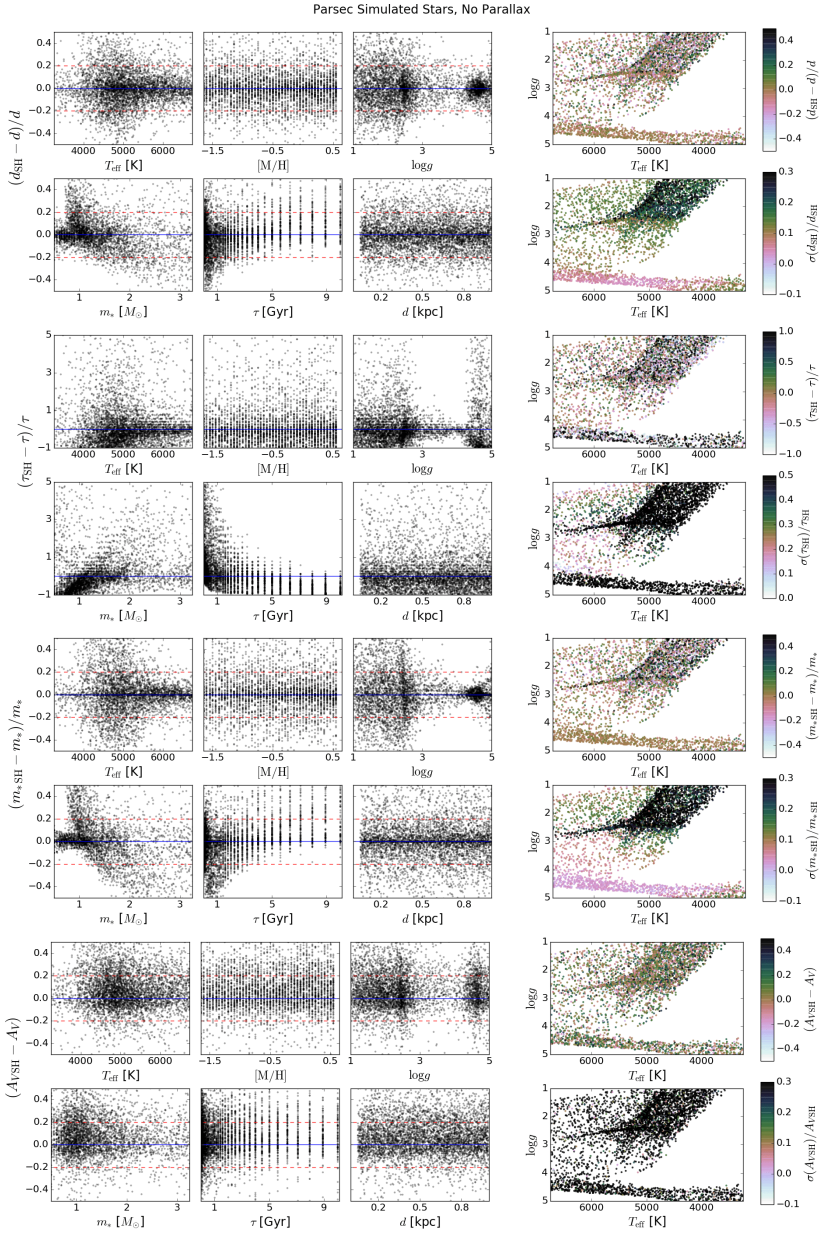

Figure A1. Same panels as in Figure 3, but now showing the results from StarHorse when the constraint provided by the parallax is not used.

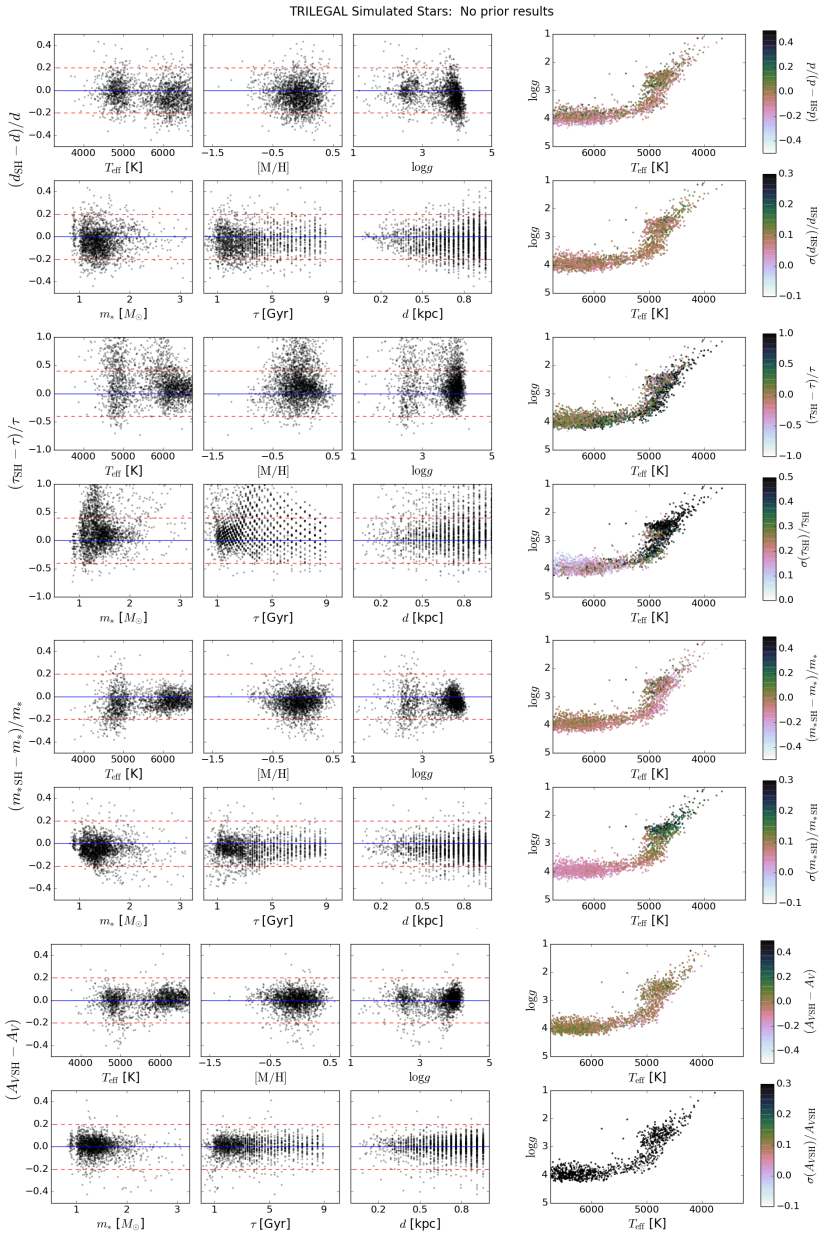

Figure A2. Same panels as in Figure 4, but now showing the results from `StarHorse` when no priors in metallicity, age and spatial distribution are adopted.

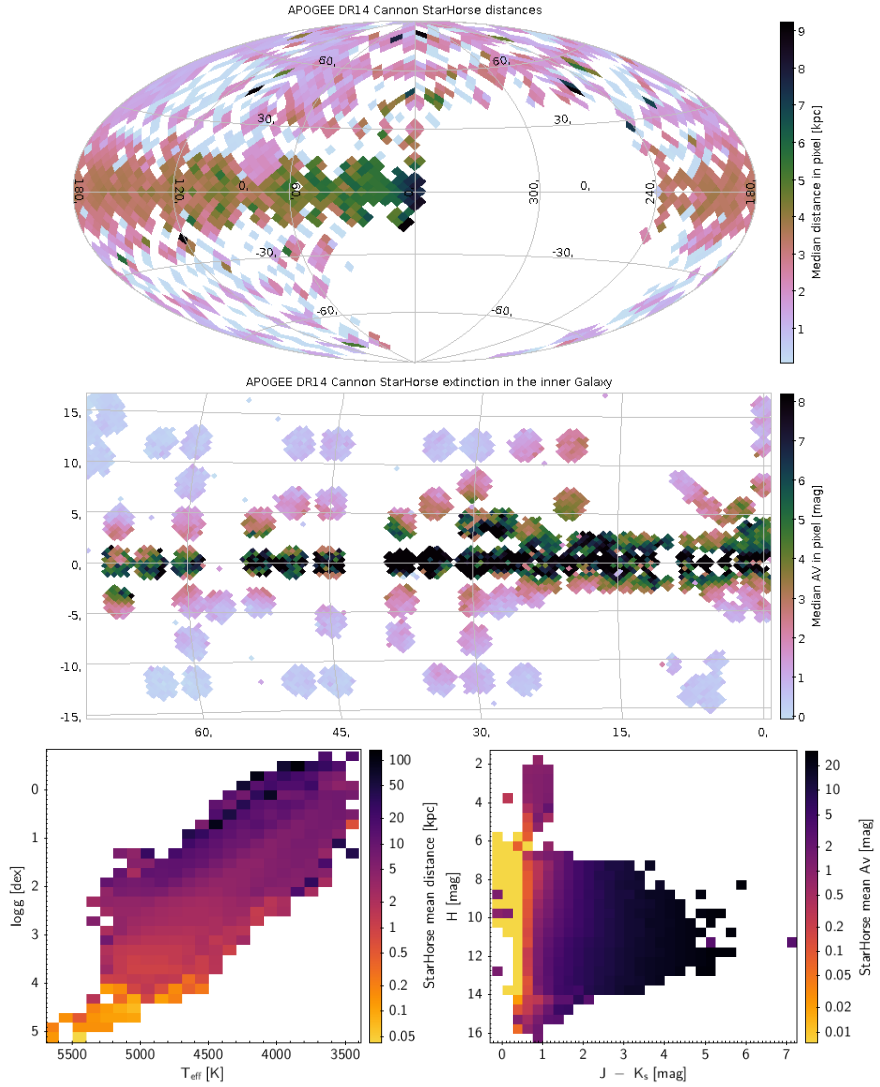

Figure B1. Illustration of the APOGEE DR14 Cannon distance and extinction results from StarHorse. The panels and conventions are the same as in Figure 11.

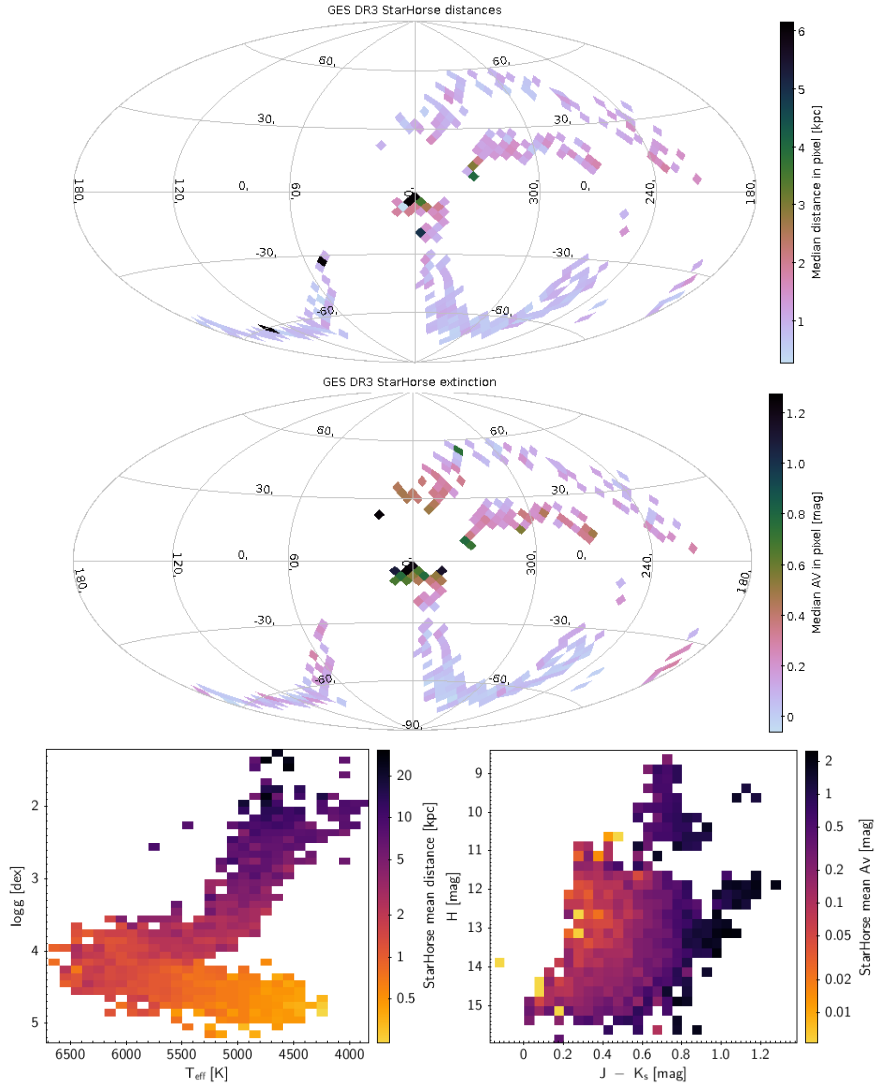

Figure B2. Illustration of the GES DR3 distance and extinction results from `StarHorse`. The panels and conventions are the same as in Figure 11.

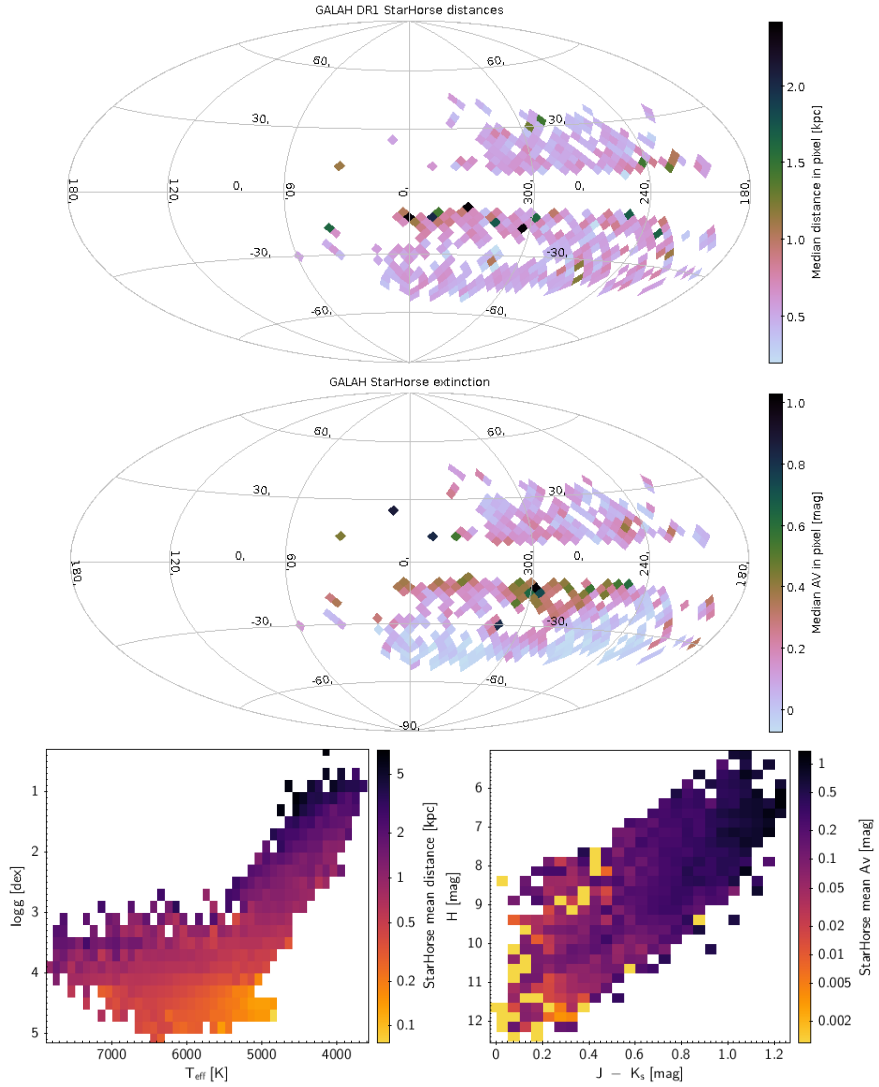

Figure B3. Illustration of the GALAH DR1 distance and extinction results from StarHorse.The panels and conventions are the same as in Figure 11.

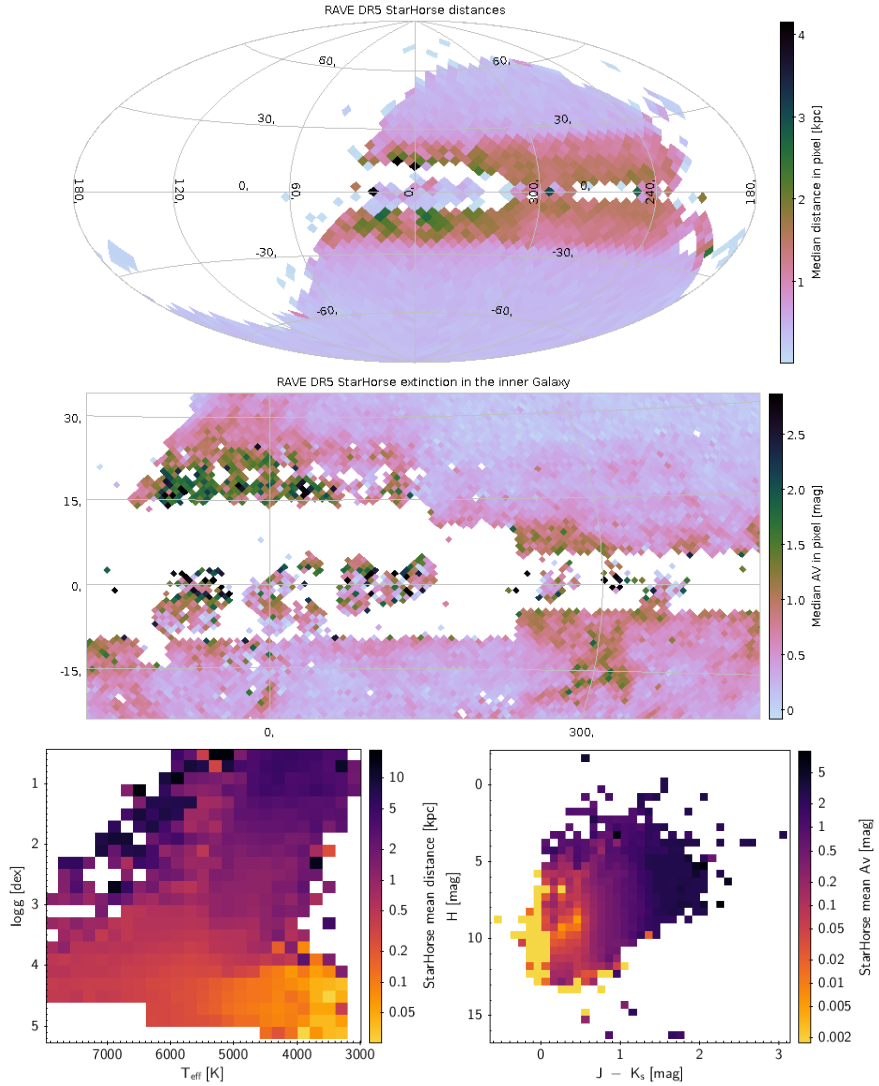

Figure B4. Illustration of the RAVE DR5 distance and extinction results from StarHorse. The panels and conventions are the same as in Figure 11.

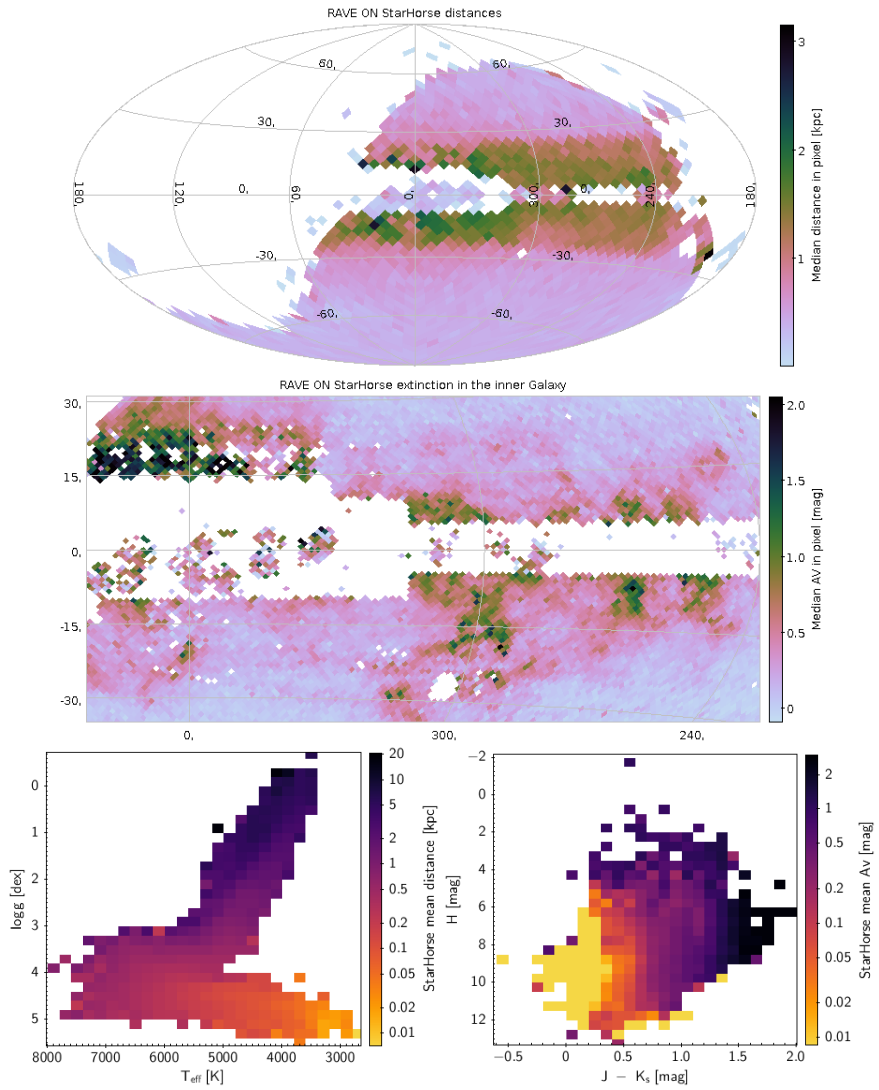

Figure B5. Illustration of the RAVE ON distance and extinction results from StarHorse. The panels and conventions are the same as in Figure 11.

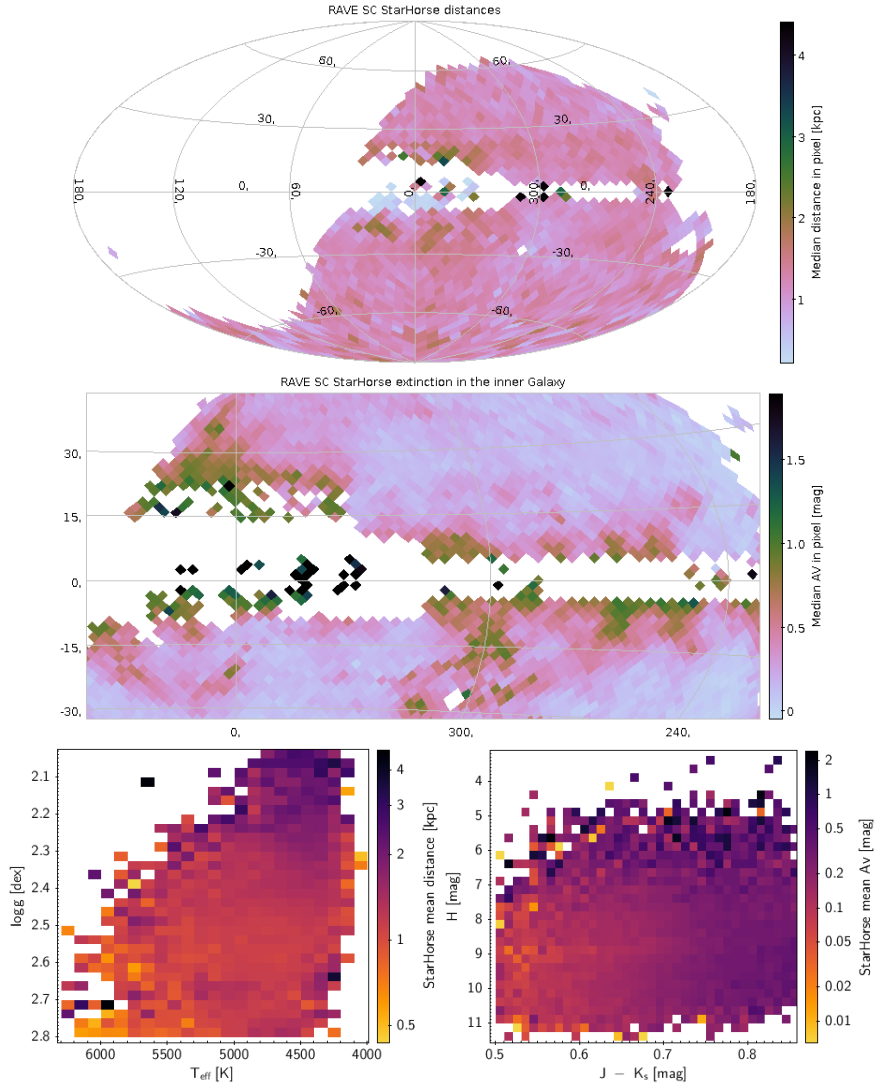

Figure B6. Illustration of the RAVE SC distance and extinction results from `StarHorse`. The panels and conventions are the same as in Figure 11.

Chapter 3

Extended analysis of APOGEE and *Gaia* samples

In this chapter, we extend the analysis of the `StarHorse` data products seen in Chapter **??**. We will qualitatively explore the value-added catalogs generated by the code to map spatial variations of stellar chemical abundances, ages, and extinction across the Galaxy. We focus on the APOGEE Survey (**?**) results, because this is the only spectroscopic survey that can peer into the dust and unveil the Galactic midplane in detail, towards bulge regions. As a results, a good estimate of extinction is crucial for this survey. We also show new results for recent *Gaia* Data Release 2 (DR2). We have recently applied the Bayesian method to matches of *Gaia* DR2 with spectroscopic catalogues such as APOGEE DR15 (this later is still restricted to the internal collaboration), and also to the full *Gaia* DR2 catalogue down to magnitudes brighter than G=18.0, where G covers the electromagnetic spectrum in the band 330–1050nm. That amounts to almost 200 million targets.

3.1 *Gaia* Mission and its Data Release 2

Gaia (**?**) is a space mission that aims to make a three-dimensional map of the Milky Way. Gaia DR2 has delivered measurements of brightness and positions for 1.7 billion stars, distances and proper motions for 1.3 billion stars, surface temperature 161 million stars, radius and luminosity for 77 million, and radial velocity for 7 million stars. That is, beyond any doubt, a revolution in stellar astronomy compared with its predecessor astrometry missions, such as *Hipparcos*, which took astrometry measurements for about 1 million stars. Furthermore, *Gaia* has a better resolution than the astrometric measurements done by *Hipparcos* (**?**). The *Gaia* DR2 data

amounts to about 1 % of the Galactic stellar population. *Gaia* has innumerable science applications in Galactic astronomy, and is expected to reveal important clues about the formation and evolution of our Galaxy. The spacecraft is operating since 2014, and the first data releases, *Gaia* DR1 (**?**) and *Gaia* DR2 (**?**) have come out in October 2017 and April 2018, respectively. *Gaia* DR1 delivered parallaxes for about two million stars, for which we have applied `StarHorse` to a combination of DR1 with several spectroscopic surveys. These are explained in detail by **?**), and some qualitative science results are shown in the next section.

3.2 Analysis of APOGEE DR14

Here we make a broad scientific analysis of the `StarHorse` results applied to the APOGEE Data Release 14 (DR14) (**?**) data combined to *Gaia* DR1. This sample was described in **?**), section 6 of Chapter **??**. In summary, we applied `StarHorse` to a match of APOGEE DR14 with *Gaia* DR1 (**?**) data and APASS (**?**). The `StarHorse` released public catalogue contains only distances and extinction values. But here we also analyse the resulting ages and masses. To study the distributions of these quantities in APOGEE DR14, we select stars with $\log g < 4.0$ and $T_{eff} < 5600$, therefore eliminating most dwarf stars contaminating the APOGEE sample. The reason for this additional cut is that dwarfs are prone to larger errors in age (**?**). We also cut the sample in distances < 10 kpc, since our estimates are degraded for larger distances. We also cut-off all negative extinction values and estimates based on a small number of models consistent with the observational data. In Figure **??** we show the HR diagram for the sample we use. The figure shows a bright horizontal branch, stars in the red giant, and a subgiant phase.

With `StarHorse` distances available, we can calculate the Cartesian Galactocentric coordinates for the stars. In Figure **??**, we show the distribution of mean ages projected on the cartesian XZ plane, where the X-axis connects the Solar position (X=8.2 kpc) to the Galactic Centre (X=0), and the Z-axis is perpendicular to the disk plane. We can see from figure **??** that the younger stars are concentrated in the disk. There is a concentration of intermediate age stars in the Solar position, probably due to the projection along the Y-axis. Older ages, $\tau > 10.0$ Gyrs, are found mainly at high Z_{gal}, beyond 5 kpcs from the disk plane, in regions mostly inhabited by halo stars. This age map is in accordance with previous Galactic age studies, also cited in the introduction of this work **????**).

In Figure **??** we show the Galactic Cartesian XZ projection colour coded by

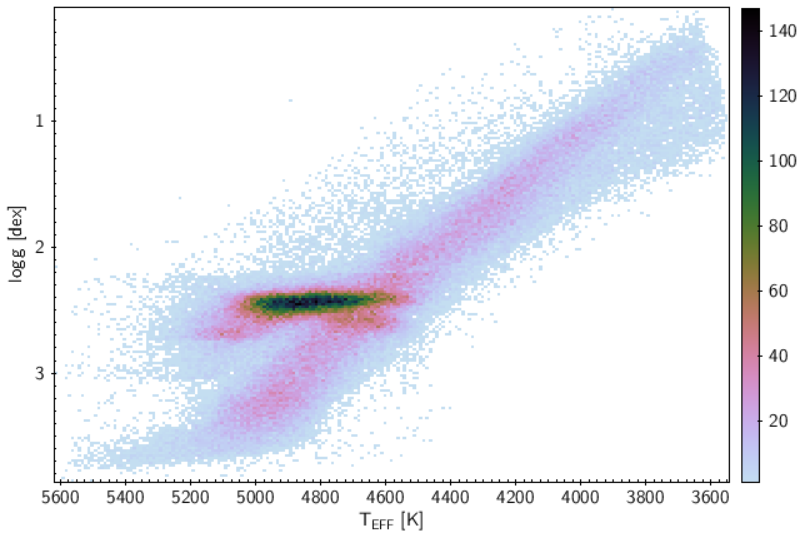

Figure 3.1: HR diagram of APOGEE DR14 sample for stars with `StarHorse` distance smaller then 10 kpc. The image is colour coded by number of stars.

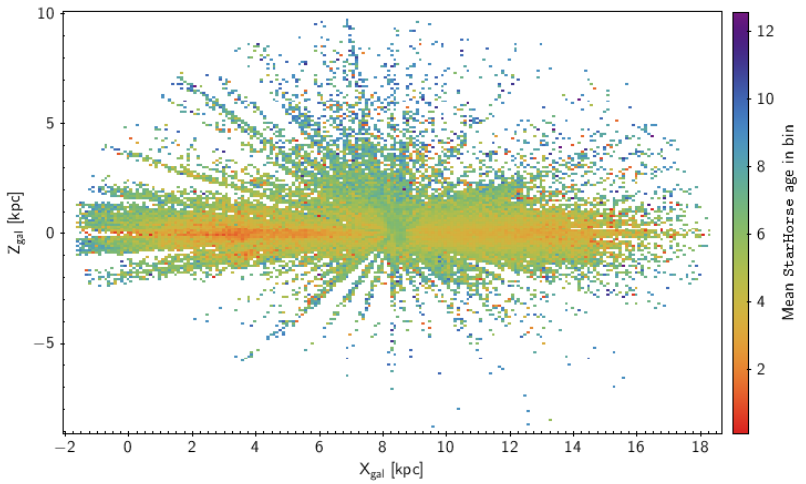

Figure 3.2: 2-D histogram of mean age values projected on XZ cartesian Galatocentric coordinates. Ages and distances were calculated by `StarHorse` distances. The vertical colour bar on the right shows the `StarHorse` ages

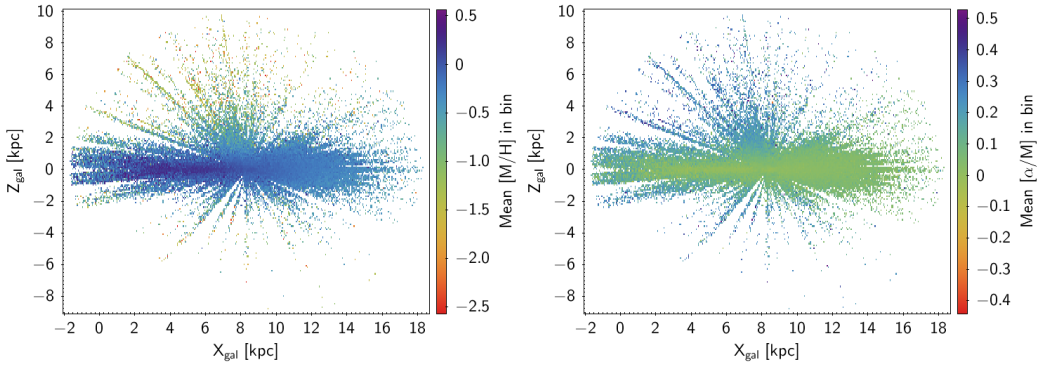

Figure 3.3: 2-D histograms of mean abundances projected on XZ cartesian Galatocentric coordinates. Distances were calculated by `StarHorse`. Left panel is colour coded by mean overall metallicity and right panel is colour coded by mean $[\alpha/M]$ abundance

mean overall metallicity, (left panel) and mean α-abundance, (right panel). According to previous works (**??**), thin disk stars have roughly Solar metallicity and low α-abundance, while thick disk stars are characterised by high α-abundance and lower metallicity. In Figure **??**, we can identify the thin disk as the dominant $\simeq$ Solar metallicity population close to the plane. We can also notice the flaring of this thin disk population towards directions away from the Galactic centre (to the right of the panels), as described by (**??**). The flaring leads to higher disk scale heights at larger distances from the Galactic center. We can also see a clear negative metallicity gradient close to the disk plane. Furthermore, the solar-like α-abundance population extends to larger distances along the disk plane than the high α-abundance population more characteristic of the thick disk, again in accordance with previous studies **??**). Since the flared out low α-abundance population at high Galactocentric radii tends to be more metal-rich than the thick disk high α-abundance seen at smaller radii, a slight positive metallicity gradient can be seen at high Z values, in agreement with **?**).

3.3 Preliminary analysis of APOGEE DR15

Now we repeat the analysis for the APOGEE Data Release 15 (DR15, still internal to the APOGEE collaboration) in combination with *Gaia* DR2. As explained in the previous section, this latter has multiplied by three orders of magnitude the number of parallaxes measurements from DR1. APOGEE DR15 has also considerably enlarged the number of targets compared with APOGEE D14, since this new data release now also includes data from APOGEE south, clearly improving the coverage

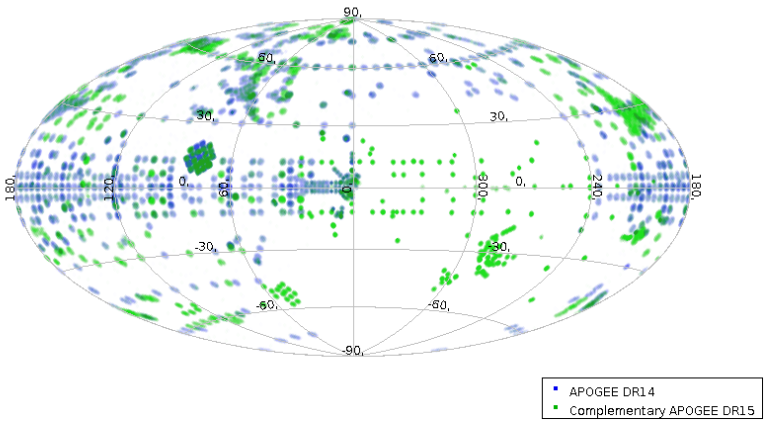

Figure 3.4: Aitoff Galactic projection showing sky coverage for APOGEE DR15 and APOGEE DR14, highlighting new targeted regions of APOGEE south.

of the bulge/inner regions that were not well sampled before, see Figure **??** showing the complementary data of APOGEE DR15 in comparison with DR14. The results we show here for APOGEE DR15 data in combination with Gaia DR2, however, must be considered as preliminary, since we are still in the process of analyzing the `Starhorse` VAC that came out of it.

In Figure **??** we see the distribution of ages for APOGEE DR15 in Galactocentric coordinates. The map is in concordance with the previous Figure **??**, though with an increase of data and sky coverage. The ages we show for these preliminary data are certainly more precise than in the previous section, since here we have available parallaxes for most of the targets. In Figure **??** we show the distribution of relative age uncertainties in the two VACs. We can see the improvement that the more precise *Gaia* parallaxes make in the uncertainty of `StarHorse` ages. We also show, in Figure **??**, the distribution of metallicity in Cartesian Galactocentric coordinates. Again the metallicity map is in agreement with the previous Figure **??** for APOGEE DR14, though covering a larger amount of data, and having more precise distances measurements.

3.4 Full Gaia DR2

Besides the APOGEE sample, we have also applied `StarHorse` to all sources of *Gaia* DR2 with mag $G < 18.0$. In Figure **??**, we show the extinction map built with `StarHorse` A_V estimates. These A_V values were calculated using as input the *Gaia* DR2 parallaxes, *Gaia* magnitudes (in the passbands G 330–1050nm, BP 330–680

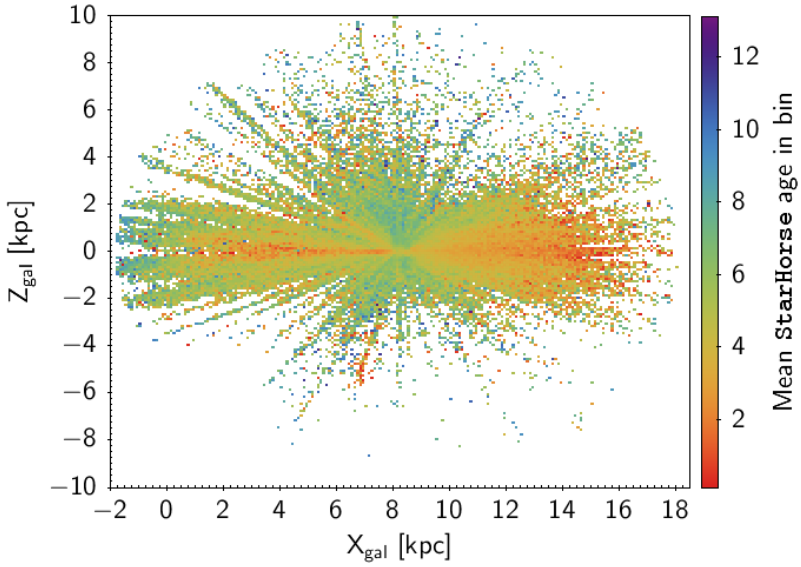

Figure 3.5: 2-D histogram of cartesian Galatocentric coordinates, calculated from `StarHorse` distances, colour coded by `StarHorse` ages for APOGEE DR15

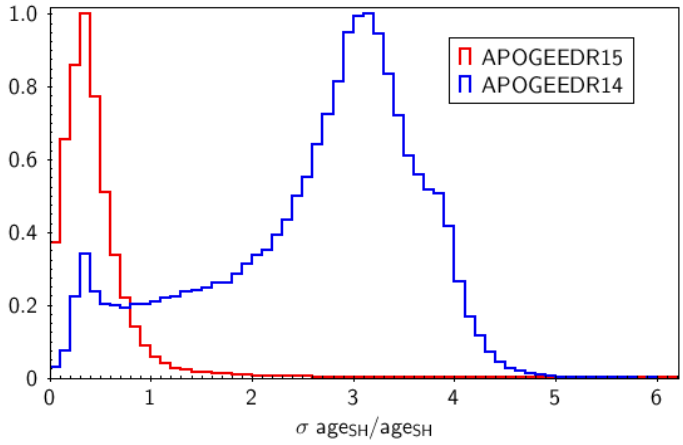

Figure 3.6: Distirbution of age uncertainties determined by `StarHorse` for APOGEE DR15 and APOGEE DR14, normalised by unit. We can see the clear improvement by using *Gaia* parallaxes.

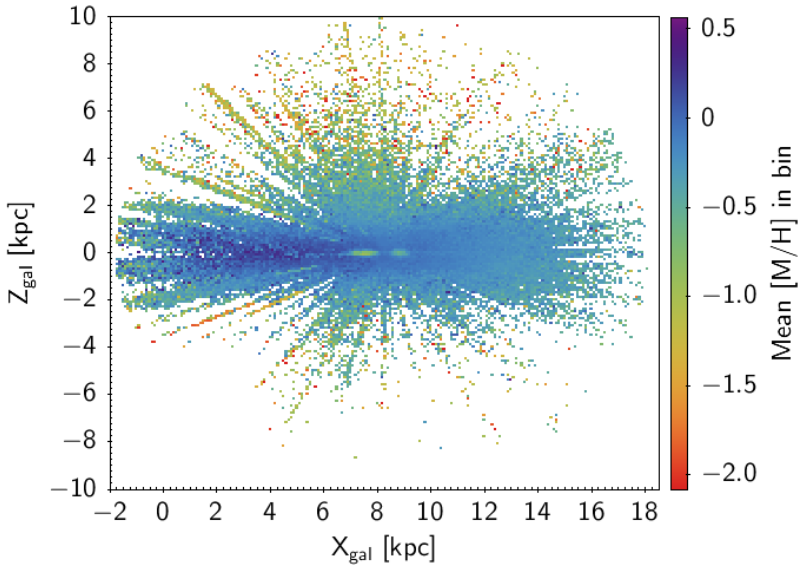

Figure 3.7: 2-D histogram of cartesian Galatocentric coordinates, calculated from `StarHorse` distances, colour coded by APOGEE DR15 $[M/H]$ abundance

nm, *RP* 640–1050 nm), and an A_g extinction values derived by *Gaia* Apsis (**?**) as A_V prior. The extinction map was built with all sources with $G<14.0$ mag and no flag cut was applied. The dust structures seen in Figure **??** are well-known dust regions of the Milky Way (e.g. Taurus and Perseus regions **??**, Ophiucus region **?**) and `StarHorse` seems to be reproducing these dust regions with a good resolution. The extinction map we show is also in good agreement with the maps produced by Apsis. In Figure **??** we zoom the extinction map in the central region of our Galaxy, which is the most obscured region. In Figure **??** we show a comparison of our distances and uncertainties with an alternative method for deriving distances (**?**). This alternative method uses only spatial Galactic priors and the *Gaia* parallaxes, we can see from Figure **??** that the distances are in good agreement, especially for small distances. We also notice from Figure **??** that our uncertainties are usually smaller, probably due to the fact we add more constrains in the distances calculations by using *Gaia* photometry.

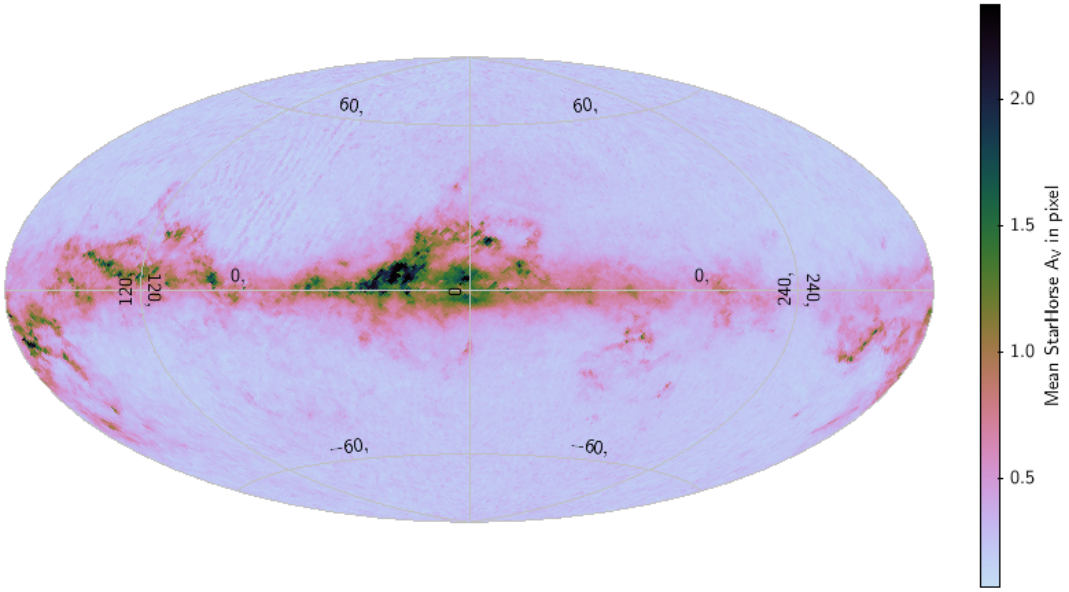

Figure 3.8: Extinction map of the Milky Way built with `StarHorse` A_V values using only Gaia photometry and parallaxes

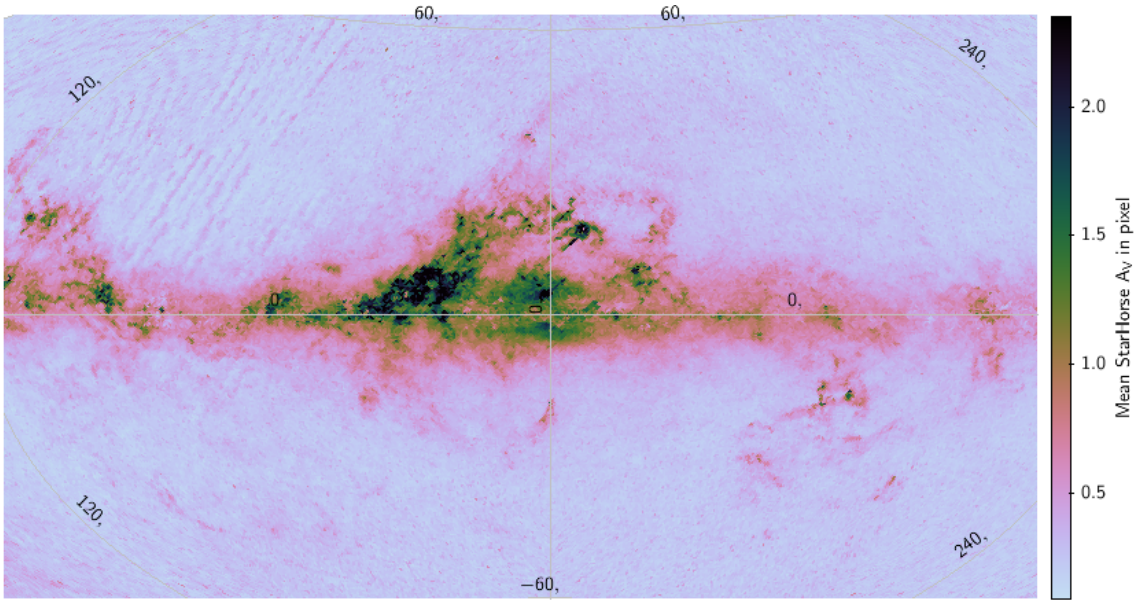

Figure 3.9: Extinction map of the Milky Way built with A_V values from `StarHorse` using Gaia photometry and parallaxes, with a zoom in to the central part of the Milky Way.

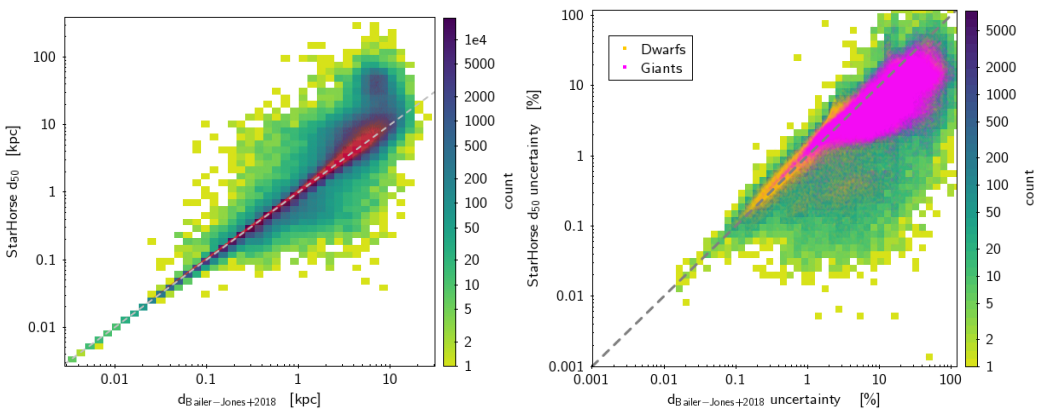

Figure 3.10: Right panel: comparison between `StarHorse` distances and **?**) distances for *Gaia* DR2. Left panel: comparison between `StarHorse` and **?**) distance uncertainties, dwarfs and giants are highlighted. Both panels are shown in logarithmic scale.

Chapter 4

Conclusions and Future Perspectives

Through this work, we have seen that `StarHorse` is a very useful tool for Galactic archaeology studies, especially in this advent of new large spectroscopic, astrometric, and photometric surveys. With `StarHorse`, we have the power to improve the precision of distances and extinction values given by *Gaia* and to infer more information about field stars, such as their ages and masses. We have presented `StarHorse` in detail in Chapter **??**. In summary, it is a Bayesian code that determines values of extinction, distance, ages, and masses for field stars, using spatial priors for each Galactic components and also metallicity and ages distributions expected for each component. We have extensively tested these priors and the code itself, using simulated sets of stars, as well as samples of real stars for which ages, masses, and distances are accurately known. VACs of large spectroscopic samples, such as APOGEE, GES, RAVE, and GALAH have also been generated and made publicly available at LIneA's website (http://www.linea.gov.br/020-data-center/acesso-a-dados-3/spectrophotometric-distances-starhorse-code/). `StarHorse` has already been used to study spatial gradients in the chemistry of the disk (**?**) and halo (**??**). Results from our code have been used to study stellar populations in the local neighbourhood (**?**), disk kinematics (**?**), disk formation (**?**), and stellar streams (**?**). Additionally, **?**) are using `StarHorse` ages, along with detailed chemical information of nearby stars, to identify statistically significant chemical and kinematical subgroups in the Solar neighbourhood.

In this work, besides presenting the code, its validation, and VACs (Chapter **??**), we have also made a qualitative analysis of spatial gradients in age, metallicity, and extinction in Chapter (**??**). For that purpose, we focused on APOGEE and on the two *Gaia* Data Releases.

In fact, the recent *Gaia* DR2 opens up a huge window of opportunities for Galac-

tic structure and stellar population studies. Still, a large potential of exploring *Gaia* data will require refining them, most especially the parallaxes. Consider the case of the Galactic bulge, as an example. A red giant of $M_G \simeq 0$ under an extinction of $A_G \simeq 2$ will have an observed apparent magnitude of $G \simeq 17$. According to **?**), the typical precision in the parallax at this S/N level will be $\simeq 0.1$ mas. At the bulge's distance of $\simeq 8$ kpc, however, this uncertainty is comparable to the parallax itself. Adding photometric and/or spectroscopic information about a sample of bulge stars to the prior info provided by the *Gaia* parallax will certainly increase the precision of the distances, hence allowing selection and analysis of a more genuine bulge sample. A similar type of reasoning also applies to the outer disk and halo, albeit with reduced S/N and scarcer spectroscopic information, as more distant samples are considered. We could also notice in Chapter **??**, the huge improvement in the resulting `StarHorse` ages by adding *Gaia* parallaxes to the spectroscopic information of APOGEE. This provides us with unique data to analyse the inner disk and bulge region, extending similar analysis made with APOGEE DR14 and *Gaia* DR1 (e.g. **?**). With these perspectives in mind, our Brazilian Participation Group at SDSS-IV, in collaboration with C. Chiappini and F. Anders, among others, at the AIP/Germany, are running `StarHorse` over the full *Gaia* DR2 sample, down to $G = 18$, with a plan to extend it over the full sample. We are also running the code on the overlapping samples between *Gaia* and the aforementioned spectroscopic surveys. These datasets, most especially APOGEE will then be used to study the inner Galactic disk and bulge regions, something that is planned for my Ph.D.